Heavy-Metal-Free Colloidal Quantum Dots: Progress and Opportunities in Solar Technologies

Lei Jin, Gurpreet Singh Selopal,* Xin Tong, Dmytro F. Perepichka, Zhiming M. Wang,* and Federico Rosei**

Colloidal quantum dots (QDs) hold great promise as building blocks in solar technologies owing to their remarkable photostability and adjustable properties through the rationale involving size, atomic composition of core and shell, shapes, and surface states. However, most high-performing QDs in solar conversion contain hazardous metal elements, including Cd and Pb, posing significant environmental risks. Here, a comprehensive review of heavy-metal-free colloidal QDs for solar technologies, including photovoltaic (PV) devices, solar-to-chemical fuel conversion, and luminescent solar concentrators (LSCs), is presented. Emerging synthetic strategies to optimize the optical properties by tuning the energy band structure and manipulating charge dynamics within the QDs and at the QDs/charge acceptors interfaces, are analyzed. A comparative analysis of different synthetic methods is provided, structure-property relationships in these materials are discussed, and they are correlated with the performance of solar devices. This work is concluded with an outlook on challenges and opportunities for future work, including machine learning-based design, sustainable synthesis, and new surface/interface engineering.

1. Introduction

Due to its relative abundance, sustainability, carbon neutrality, and cost-effectiveness, solar energy stands out as a promising renewable energy source. The Earth receives solar radiation of ≈173 000 terawatt hours (TWh) per hour, capable of satisfying global energy consumption annually.[1] By harnessing solar radiation and converting it into usable forms such as electricity and clean chemical fuels, our dependence on limited fossil fuels can be decreased through advanced sustainable energy practices.[2] Semiconductors play a crucial role in solar-electrical or solar-chemical energy conversion, serving as photoabsorber materials that absorb photons, generate excitons (electron-hole pairs), and facilitate charge separation.[3] Colloidal quantum dots (QDs), which are semiconductor nanocrystals capped with surfactant molecules,[4] offer advantages such as solution processing and quantum confinement, allowing precise modulation of their optoelectronic properties by adjusting their size and shape without altering chemical bonds.[3,4] With a broad absorption range (300–2000 nm) and large absorption cross-sections, QDs demonstrate excellent solar-light harvesting capabilities. The potential for multiple exciton generation (MEG)[5] and hot-electron extraction before thermalization[6] raises the prospect of exceeding the Shockley-Queisser limit of 32.7%[7] in the PCE of single-junction photovoltaic (PV) devices. Combined with their abundant surface binding sites, high photoluminescence quantum yield (PLQY), and straightforward surface functionalization, colloidal QDs are increasingly employed in solar energy conversion technologies, including PV devices,[8] solar-driven fuel production (e.g., H_2 generation, CO_2 photoreduction)[9] and luminescent solar concentrators (LSCs).[10] Notable achievements include the development of a PbS QD-based photoelectrochemical (PEC) cell with a peak external quantum efficiency (EQE) exceeding 100% for PEC H_2 evolution reactions,[5a] a quantum

L. Jin
Centre for Energy
Materials and Telecommunications
National Institute of Scientific Research
1650 Boul. Lionel-Boulet, Varennes, QC J3X1P7, Canada
E-mail: jin.jin@mail.mcgill.ca

L. Jin, D. F. Perepichka
Department of Chemistry
McGill University
801 Sherbrooke Street West, Montreal, QC H3A 0B8, Canada

G. S. Selopal
Department of Engineering
Faculty of Agriculture
Dalhousie University
39 Cox Rd, Banting Building, Truro, NS B2N 5E3, Canada
E-mail: gs.selopal@dal.ca

X. Tong, Z. M. Wang
Shimmer Center
Tianfu Jiangxi Laboratory
Chengdu 641419, P. R. China
E-mail: wangzhiming@jxl.ac.cn

F. Rosei
Department of Chemical and Pharmaceutical Sciences
University of Trieste
Via Giorgeri 1, Trieste 34127, Italy
E-mail: federico.rosei@inrs.ca

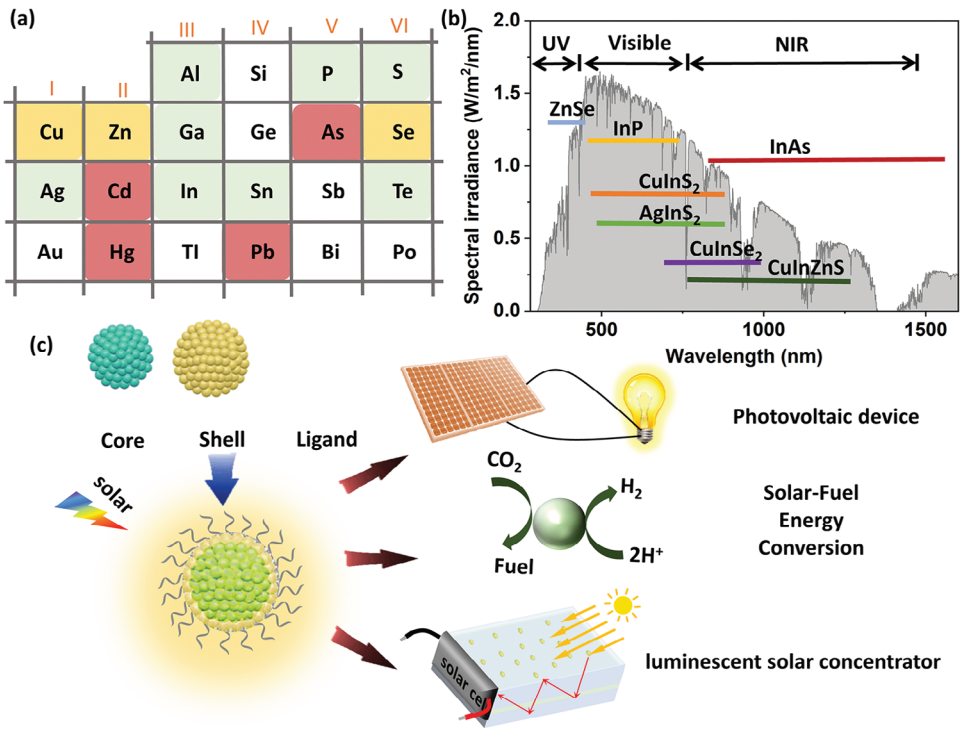

Figure 1. a) The elements commonly utilized in QDs are depicted in colors that indicate their toxicity levels. Red signifies highly toxic, yellow denotes non-toxic at small amounts but highly toxic at high doses, and green shows relatively non-toxic. b) The solar spectrum (AM 1.5G, 100 mA cm^{-2}, grey area) and optical spectra range of some representative heavy-metal-free QDs. c) Colloidal core/shell QDs and their solar applications: solar cells, solar-chemical fuel conversion, and LSCs.

efficiency (QE = $2N_{H2}/N_{h\nu}$, where N_{H2} is the number of electrons per sec and $N_{h\nu}$ is the number of photons per sec) of 100% for PEC cells based on Pt-tipped CdSe/CdS QDs,[11] a certified PCE of 18.1% for perovskite QD-based solar cells,[12] and unprecedented optical efficiencies of LSCs based on CdSe/CdS,[13] CdSe/$Cd_{1-x}Zn_xS$,[14] and PbS/CdS QDs.[15] However, the presence of hazardous metal contents (e.g., Pb or Cd) in most high-quality QDs is a major unresolved challenge,[16] severely limiting their commercial-scale applications.

Since the 1990s, there has been consistent advancement in the fabrication of heavy-metal-free QDs,[17] which are composed of elements lacking certain toxic heavy metal elements, including Cd, Pb, Hg, and As etc. (**Figure 1a**). **Table 1** lists the representative heavy-metal-free QDs for solar energy conversion. Recent efforts have improved our understanding of these systems, including studies on surface chemistry,[18] electron and hole relaxation,[19] the distribution of trap states,[20] and the origin of PL emission in binary[21] and ternary[22] QDs. However, the heavy-metal-free QDs are still in their early developmental phases, with their overall efficiency in solar energy conversion trailing behind that of Pb- and Cd-based counterparts. Pb- and Cd-based QDs boast advantageous bandgap characteristics and superior optoelectronic properties, including broad light absorption extending into the infrared spectrum, narrow emission spectra, high PLQY, and unique band alignment conducive to efficient carrier dynamics. Consequently, the synthesis of Pb- and Cd-based QDs has undergone extensive research over several decades, involving meticulous material selection, advanced surface passivation techniques, and optimization of synthesis protocols. Conversely, the synthesis techniques of heavy-metal-free QDs are still at an early stage of development, necessitating further optimization. Additionally, a significant knowledge gap exists regarding the intricate mechanisms underlying the synthesis of heavy-metal-free QDs and their optical/electronic properties. Furthermore, integrating heavy-metal-free QDs into optoelectronic devices requires compatible device architectures and processing methodologies. In this context, several outstanding challenges are in need to be addressed for heavy-metal-free QDs: i) enhancing the light-harvesting capability of QDs to better align with the solar spectrum (Figure 1b); ii) improving charge separation at QDs/charge acceptor interfaces; iii) facilitating charge transfer/transport for conversion of solar energy into electricity or clean fuels; iv) separating the absorption and emission spectra to eliminate the self-absorption energy loss; v) minimizing the undesirable non-radiative charge recombination; vi) enhancing the long-term stability of QDs. To address these challenges, substantial efforts were concentrated on improving the optical properties of QDs,[23] crafting cooperative downshifting layers to bolster light absorption,[24] and formulating surface ligands to simultaneously enhance charge extraction and ensure the prolonged stability of QDs.[25]

The last decades have witnessed a surge of publications on heavy-metal-free QDs and related solar technologies,[26] prompting a critical review of this field to identify outstanding challenges and opportunities. Several review articles focused on synthesizing colloidal QDs using wet-chemistry approaches and their

Table 1. Representative heavy-metal-free colloidal QDs for solar energy conversion.

Classification		Materials	Abs edge [nm][b)]	PL peak [nm][b)]	PL QY [%]	Application	Merits	Challenges
Binary QDs	C[a)]	Ag_2S	670/1250	690/1270	50	PV[29]	Consist of only two distinct elements, simplify the synthesis and characterization Better size and compositional uniformity The crystal structure is simpler and more stable	Limited tunable range of light absorption and emission Restricted selection of elements Susceptible to blinking and photo-bleaching
		Ag_2Se	690/1320	700/1330	65	PV[30]		
		ZnSe	360/435	370/445	60	PV[31]		
		InP	410/700	420/710	93	CO_2RR[32]		
	C/S[a)]	Ag_2S/ZnS	410/950	420/960	5	PV[33]		
		InP/ZnS	420/790	430/800	90	PC[25b]		
		InP/ZnSe	470/620	480/630	90	PEC[34]		
		InP/ZnO	580/620	590/630	30	LSC[35]		
		SnSe/ZnSe	800/1000	–	–	PEC[36]		
	C/S/S[a)]	InP/Gap/ZnSe	580/650	590/660	72	PEC[37]		
Ternary QDs	C	$CuInS_2$	680/830	690/840	80	PC[38]	Expanded tunability with compositional control Wider absorption range Large Stokes Shift Reduced blinking	Complex synthesis Difficult in precise control over the composition Difficult in achieving size homogeneity Potential interdiffusion effects
		$CuInSe_2$	450/1140	460/1150	28	PV[39]		
		$AgInS_2$	415/800	425/820	36	CO_2 RR[40]		
		$AgBiS_2$	1000/1200	530/550	–	PV[41]		
	C/S	$CuInS_2$/ZnS	600/810	550/920	90	LSC[42]		
		$CuAlS_2$/ZnS	670/810	680/920	3	PV[43]		
		$AgInS_2$/ZnS	500/820	550/920	83	PV[44]		
		$AgInSe_2$/ZnS	690/810	700/820	40	PEC[45]		
		$AgInSe_2$/ZnSe	600/800	650/810	–	PEC[46]		
		$CuInSe_2$/ZnS	600/810	610/820	23	PV[47]		
		$CuInSe_2$/$CuInS_2$	1090/1100	1090/1100	2	PEC[48]		
	C/S/S	$CuInSe_2$/CuInSeS/$CuInS_2$	1075/1100	1075/1100	–	PEC[23]		
		$AgInSe_2$/AgInSeS/$AgInS_2$	790/900	800/910	4	PEC[49]		
Quaternary QDs	C	Zn-Cu-In-Se	550/1000	570/1020	4	PV[50]		
		Zn-Cu-In-S	500/1000	530/1030	1	PV[51]		
		Ag-Zn-In-S	470/640	480/650	32	PC[52]		
		CuInSSe	760/1100	780/1120	5	PEC[53]		
		CuInGaSe	600/1000	650/1100	–	PV[39]		

(*Continued*)

Table 1. (Continued)

Classification		Materials	Abs edge [nm][b)]	PL peak [nm][b)]	PL QY [%]	Application	Merits	Challenges
		Cu_2ZnSnS_4	688/826	–	–	PV[54]		
	C/S	CuGaAlS/ZnS	400/450	478/578	91	LSC[55]		
		CuGaInS/ZnS	600	630	95	LSC[56]		
		CuAgInS/ZnS	620	630	–	PEC[57]		
		ZnCuInS/ZnS	450/650	570/720	26	PV[58]		
		ZnCuInSe/ZnSe	680/820	690/830	65	PV[59]		
Quinary QDs	C	Zn-Cu-In-S-Se	790/820	800/830	65	PV[60]		
Doped QDs	Doped C	Zn,Al:$CuInS_2$	800	734	–	LSC[61]	Dopants can modify the electronic and optical properties, enabling new functionalities.	Challenges in achieving uniform doping and controlling dopant distribution Dopant-induced defects may affect the stability and performance of QDs
	Doped C/S	Cu:InP/ZnSe	600/750	630/790	40	LSC[62]		
		Cu:InP/ZnS	590/700	600/710	66	PC[63]		
		Cu:ZnInSe/ZnS	650/690	660/700	63	LSC[64]		
		Mn:$CuInS_2$/ZnS	640/790	650/800	–	PEC[65]		
		Mn:$CuInSe_2$/ZnSe	640/790	650/800	–	PEC[66]		
	Doped-C/Doped-S	Mn:$AgInS_2$/Cu:ZnS	700	710	–	PEC[67]		
		Cu:AgInSe/Cu:ZnSe	700	720	–	PEC[68]		

[a)] C refers core, C/S refers core/shell; C/S/S refers core/shell/shell; [b)] Before "/" represents the shortest obtainable wavelength, and after "/" represents the maximum obtainable wavelength.

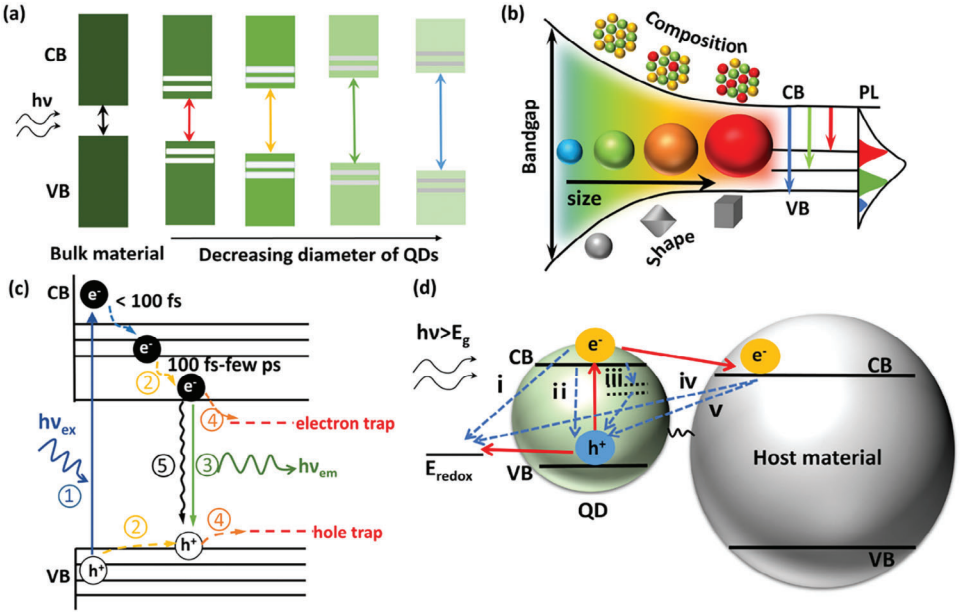

Figure 2. Schematic illustration of a) size-tunable band structure of the QDs. b) Schematic diagrams represent exciton generation and possible charge recombination in QDs as light emitters (such as in LSCs). The numbers in (c) indicate the various major photophysical processes taking place in QDs: (1) excitation upon photon absorption; (2) hot carrier relaxation to form exciton; (3) radiative decay to emit a photon; (4) carrier (electron or hole) trapping; (5) non-radiative decay. c) Representative parameters to tune QDs. d) Schematic illustrations of the possible charge transfer processes occurring at the interfaces for solar technologies using QDs as light absorbers (such as in PV, PC, and PEC systems). Numbers represent charge recombination processes: (i) electrons in the CB of QDs recombine with the oxidized species of the redox couple electrolyte at the QDs/electrolyte interface; (ii) direct charge recombination of photogenerated electrons in the CB of QDs with holes in the VB of QDs; (iii) charge recombination through intra-band surface trap/defect states within QDs; (iv) the injected electrons in the CB of the host materials recombine with the oxidized species of the redox couple electrolyte at host materials/electrolyte interface; and (v) electrons back transfer from the CB of host materials to the VB of QDs and recombine with the holes at the QDs/host-material interface.

applications,[26a,27] yet an in-depth discussion of heavy-metal-free materials and processes for solar technologies is still lacking. Progress on the applications of colloidal QDs in solar technologies was previously summarized,[4,8b,10,26b,28] while heavy-metal-free QDs were summarily discussed as only a subcategory of QDs. Until now, only three reviews have focused on heavy-metal-free colloidal QD-based solar technologies.[26] You et al. and Li et al. discussed the challenges and perspectives of developing heavy-metal-free for LSCs[26b] and PEC H_2 generation.[26c] Jain et al. summarized the synthesis, characterization, and applications of I-III-VI_2 QDs,[26a] focusing only on one specific family of heavy-metal-free QDs and their biomedical applications.

Here, we comprehensively review heavy-metal-free colloidal QDs in solar technologies, categorized as PV devices, photocatalysis (PC)/PEC systems for solar to-fuel conversion, and LSCs (Figure 1c). We initiate our discussion by systematically elucidating the distinctive characteristics of heavy-metal-free QDs, which include their tunable band structure, optical properties, and charge dynamics. This exploration encompasses the engineering of the core, shell, interfacial layer, shape, and surface of the QDs. Notably, we underscore the significance of band alignment in dictating the charge dynamics within the QDs and at the interfaces between the QDs and charge acceptors, establishing a direct correlation with device performance. We critically appraise diverse synthetic methodologies employed in fabricating heavy-metal-free colloidal QDs. Subsequently, we critically evaluate recent advancements in solar technologies leveraging heavy-metal-free colloidal QDs, highlighting the most promising strategies and accomplishments. Additionally, we delineate burgeoning opportunities within this realm and furnish perspectives for future research endeavors.

2. Tunable Design of Heavy Metal-Free Colloidal QDs

In semiconductors, the high density ($\approx 10^{22}$ cm^{-3}) of covalently/ionically bonded atoms creates a high concentration of continuous electronic states, characterized by a fully occupied valence band (VB) and an empty conduction band (CB) separated by an energy bandgap (E_g) devoid of any allowed states (**Figure 2a**). In most solar technologies, the initial step is the absorption of photons with energy above the E_g. Electrons are excited from VB to CB, and holes are left in VB, forming excitons with a characteristic exciton Bohr radius (Figure 2b).[69] The dimensions of QDs are at or below the exciton Bohr radius of the corresponding bulk materials,[70] inducing the discretization of energy levels near band edges.[70] This quantum effect gives QDs an additional degree of tunability compared with bulk semiconductors, e.g., the QD's bandgap increases as its size decreases (Figure 2c).

After light excitation of QDs, the electrons and holes relax into the bottom of the CB, and the top of the VB (thermalization) happens on a timescale of picoseconds.[71] Subsequently, electrons and holes undergo recombination processes to release energy in a radiative relaxation of band-edge excitons. The consequent

narrowband and bright emission are interesting for employing QDs as light emitters for solar applications such as LSCs. Alternatively, the electrons and holes of QDs are separated and injected into corresponding charge acceptors to continuously participate in the subsequent reduction and oxidation reactions in QD-based PC/PEC systems (Figure 2d).

Despite the advantages of QDs, the high surface-to-volume ratio of QDs leads to a significant proportion of uncoordinated atoms on the surface, resulting in heightened sensitivity.[70] This challenge can be addressed by encapsulating QDs with inorganic semiconductor shells, providing a protective environment that reduces surface charge/exciton trapping and mitigates QD degradation.[8b] Core/shell QDs not only inherit the standard features of QDs but also present an additional benefit as their energy-band structure can be finely tuned by engineering the core/shell materials, optimizing core size/shell thickness, and regulating interfacial layers.[72] The precise and systematic tunability of their optical properties provides core/shell QDs advantages in solar technologies because: a) their light absorption spectra can be adjusted for optimal spectral overlap with the solar spectrum; b) the radiative channels of QDs can be modulated to obtain a suitable PL range; c) the band structure of QDs can be tuned suitable for charge injection to electron/hole acceptors. Here, we mainly discuss the possible engineered functionalities of QDs (with special attention given to core/shell QDs) and correlate the QDs' structures with their optical properties and charge carrier dynamics for solar technologies.

2.1. Regulating the Composition of QDs

Based on the particle-in-a-sphere model of QDs, electronic energies are significantly influenced by the effective exciton mass,[73] making the composition critical for the band structure of QDs. For binary QDs composed of only two elements, doping in QDs offers opportunities to tailor their electronic and optical properties,[74] such as improving PL emission efficiency,[75] broadening the PL/absorption range to the visible (400 nm $< \lambda <$ 700 nm) or near-infrared (NIR) region (700 nm $< \lambda <$ 1700 nm),[17e] and protecting host QDs against photo-oxidation.[76] Typically, doping involves manipulating the constituent stoichiometries while preserving the symmetry and quality of the lattice. The most common strategy for doping is to include the dopant-contained precursors in the synthesis of host QDs. However, controlled doping remains challenging because the host matrix tends to expel specific strain-inducing dopant ions from the internal crystal lattice to the surface.[77] To overcome this challenge, nucleation-doping and growth-doping in high-temperature organometallic synthesis were developed,[78] making it possible to dope various transition metals and rare-earth ions, including Mn^{2+},[79] Cu^{2+},[80] Ag^{+},[81] Co^{2+},[82] Gd^{3+},[83] and Eu^{3+}.[84] The emission tunability of dopants on QDs highly depends on emission dynamics. For instance, the incorporation of Cu or Ag dopants can introduce an intra-gap trap state (**Figure 3a**),[17e,64,80b] resulting in light emission from the recombination of delocalized electrons in the host QDs and holes localized on the Cu or Ag ions, such as Cu:InP.[34] In Mn-doped QDs (Figure 3b), a $^6A_1$ ground state and $^4T_1$ excited states of doped Mn^{2+} are located inside the CB-VB energy gap of host QDs (Figure 3b).[76,85] A small amount of Mn^{2+} incorporated into the host QDs lattice can result in an apparent $^4T_1$-$^6A_1$ PL emission.[86] However, the emission range of Mn-doped QDs is typically limited to the 580–610 nm spectral range, with a low PLQY resulting from a non-radiative Shockley-Read-Hall (SRH) recombination process at the surface or internal defects of QD.[87] In this view, simultaneous doping of multiple dopants is an effective strategy,[88] where the overall PL emission can span over a broad spectral range by combining the intrinsic emission of the host QDs and the dopant emission. For instance, in the case of Cu and Mn ions co-doped $ZnInS_2$ QDs, the dopants retain their emissions, and a tunable spectral distribution/emission color can be realized through the variation of the Mn-to-Cu concentration ratio, enabling pure white light generation (Figure 3c).[88] The above discussion is for the doped core of QDs while doping in shell provides additional adjustment of core/shell QDs. For example, doping Cu in the ZnS shell of InP can provide charge trap sites in the shell for efficient capture of the photoexcited holes, consequently facilitating the charge separation process.[34,63]

Besides, alloying endows QDs with additional composition-dependent properties that can complement quantum confinement effects (Figure 3d).[89] For instance, to realize NIR emission in the 800–2500 nm range, InP (bulk bandgap is ≈1.29 eV) QDs need to be larger than 6 nm, and InAs (bulk bandgap is ≈0.36 eV) need to be smaller than 2 nm, both of which are synthetically challenging. In contrast, $InAs_xP_{1-x}$, an alloy of InP and InAs, can efficiently emit light in the NIR window with a reasonable size of 3.5–4.2 nm.[90] An increasing Ga concentration in InP QDs (bulk E_g: InP 1.29 eV, GaP 2.27 eV) leads to continuously blue-shifted absorption and PL peaks compared to InP,[91] indicating a tunable bandgap in the alloyed QDs. In addition, the alloyed core or alloyed shell can reduce the reconstruction-induced interfacial stain in core/shell QDs (Figure 3e).[92] For instance, InP was alloyed with Zn in the form of In_xZn_yP core,[92a] compressing the lattice constant from 5.93 Å (InP) to 5.39 Å (In_xZn_yP) by simply varying the concentration of the Zn precursor. Besides, alloying in the shell can achieve better stability and charge transfer behavior.[93] For example, adding a composition gradient ZnSeS alloyed shell on the InP core achieved the PLQY approximately twice that of InP/ZnS QDs (30%) and InP/ZnSe QDs (25%).[93]

Unlike binary QDs, multinary QDs incorporate at least three different elements, offering additional degrees of freedom for tuning their properties. Changing the ratio of elements can shift the energy levels of the QDs, altering their absorption and emission spectra with similar size (Figure 3f),[94] e.g., Ag/In for $AgInS_2$/ZnS QDs[95] and Cu/Zn for Cu-Zn-In-S QDs.[96] Adding additional elements can further tune the optical properties. For example, the PL wavelength range of $CuInS_2$ (limited to ≈1000 nm[97]) can be extended to 1210 nm by alloying with Se.[98]

2.2. Engineering the Type of Core/Shell QDs

The band alignment at the core-shell interface is crucial in core/shell QDs' emission dynamics and charge transfer behavior. Based on the core-shell band alignment, core/shell QDs are mainly defined into four categories:[9] Type-I, Reverse Type-I, Type-II, and Quasi-Type-II (**Figure 4a**).

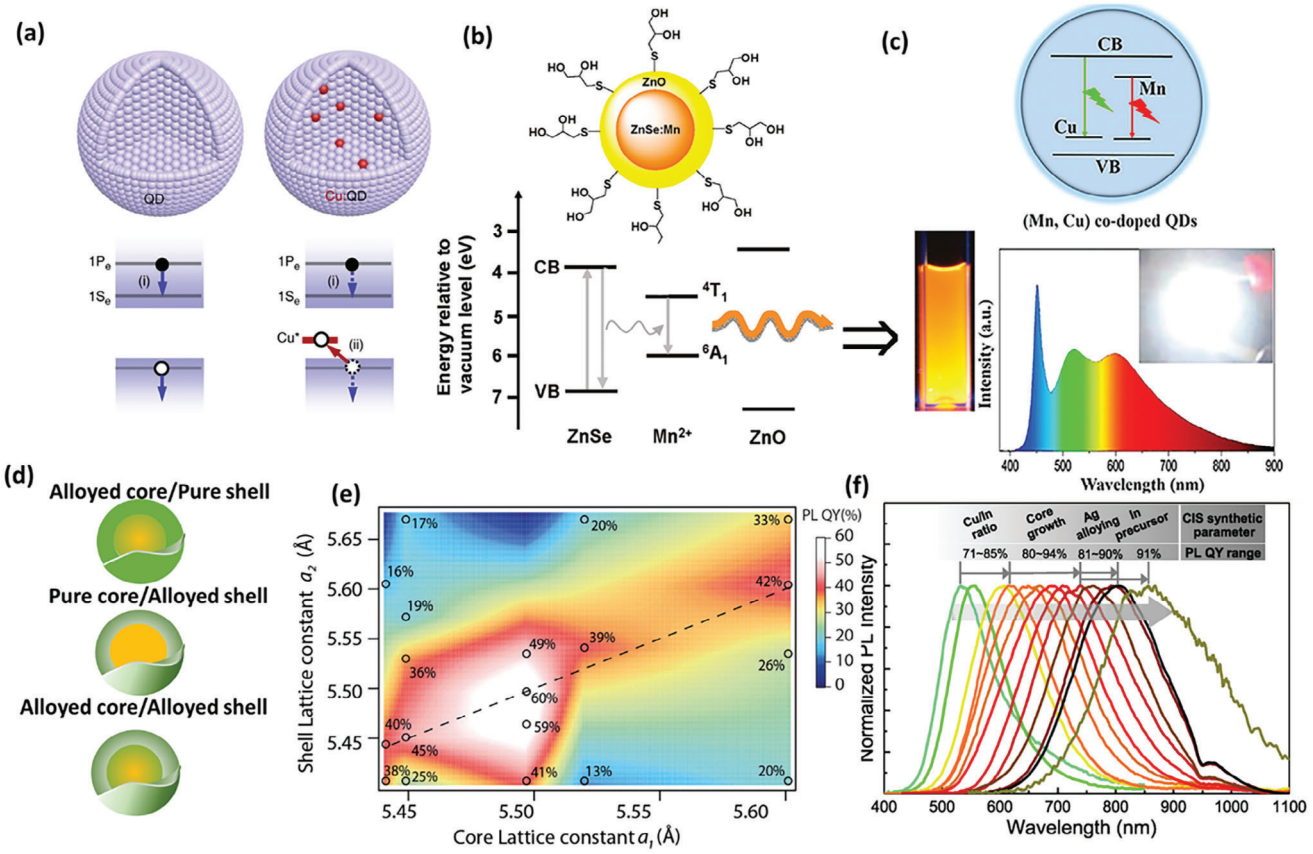

Figure 3. a) Illustration of hot electron cooling in QDs without (left) and with (right) Cu-dopant. Reproduced with permission.[99] Copyright 2019, The Authors. b) The transition from the Mn^{2+} $^4T_1$ state to the $^6A_1$ state results in orange light emission for ZnSe: Mn/ZnO core/shell QDs. Reproduced with permission.[100] Copyright 2011, American Chemical Society. c) Co-doping of Mn and Cu in ZnInS QDs for tuning the PL emission. Reproduced with permission.[88] Copyright 2015, American Chemical Society. d) Illustration of possible alloyed core/shell QDs. e) The color plot of the PLQY as a function of the lattice constants of In_xZn_yP core and $ZnSe_zS_{1-z}$ shell (right). Reproduced with permission.[92a] Copyright 2016, American Chemical Society. f) PL variation with the synthesis parameters of $CuInS_2$ QDs. Reproduced with permission.[101] Copyright 2019, American Chemical Society.

In Type-I QDs, the core's CB and VB edges lie within the band gap of the shell. Consequently, both electrons and holes are confined within the core region. The improved surface passivation may decrease trap density, leading to a high PLQY (≈60–90%) and stability.[24] However, due to charge carrier confinement, the exciton recombination is mainly controlled by the band structure of the core, leading to a significant absorption/emission spectra-overlap for self-absorption energy loss.[24] Besides, the shell establishes an energy barrier for charge tunneling, increasing the likelihood of recombination of undesired charge.[102] Except in small-sized Type-I QDs with an extremely thin shell (0.1–0.3 nm),[103] the charge separation rate typically shows an exponential decrease with the increase in shell thickness (Figure 4b).[102] A viable strategy to overcome the charge confinement of Type-I QDs is to reduce the offset between the CB of the core and the shell by alloying with other elements (such as Mn[65]), facilitating a partial electron delocalization in the shell.

In Reverse Type-I QDs, the bandgap of the core is wider, and both the CB and VB band edges of the shell are located between the bandgap of the core (Figure 4c). This energy-level alignment results in partial or complete (depending on the shell thickness) delocalization of electrons and holes in the shell region.[104] It favors the extraction of photogenerated charges and enhances the charge injection rate from QDs to charge acceptors in solar applications including PVs or PC.[105] The light emission of Reverse Type-I QDs mainly comes from the radiative recombination of the electron-hole pairs in the shell. In contrast, the shell's lack of effective charge confinement typically induces issues similar to the plain core, e.g., a relatively low PLQY (≈10%)[104] and poor photostability. In this case, a secondary Type-I shell, an energy barrier hindering electron trapping at the surface trap states, can enhance light emission.

In Type-II core/shell QDs, either the CB or VB of the shell is located in the core's bandgap (Figure 4d). The small overlap between the wave functions of electrons and holes reduces their Coulombic interaction,[106] inducing spatial separation of electrons and holes in core and shell,[105] e.g., one carrier is confined in the core. At the same time, the other one is mainly located in the shell. The effective bandgap (PL emission) of Type-II core/shell QDs primarily depends on core and shell band offset (energy gap between shell CB and core VB or between core CB and shell VB).[106] As a consequence, the PL wavelength is red-shifted compared to that of plain core QDs. The CB (or VB) band energy offset between the core and shell can be adjusted by

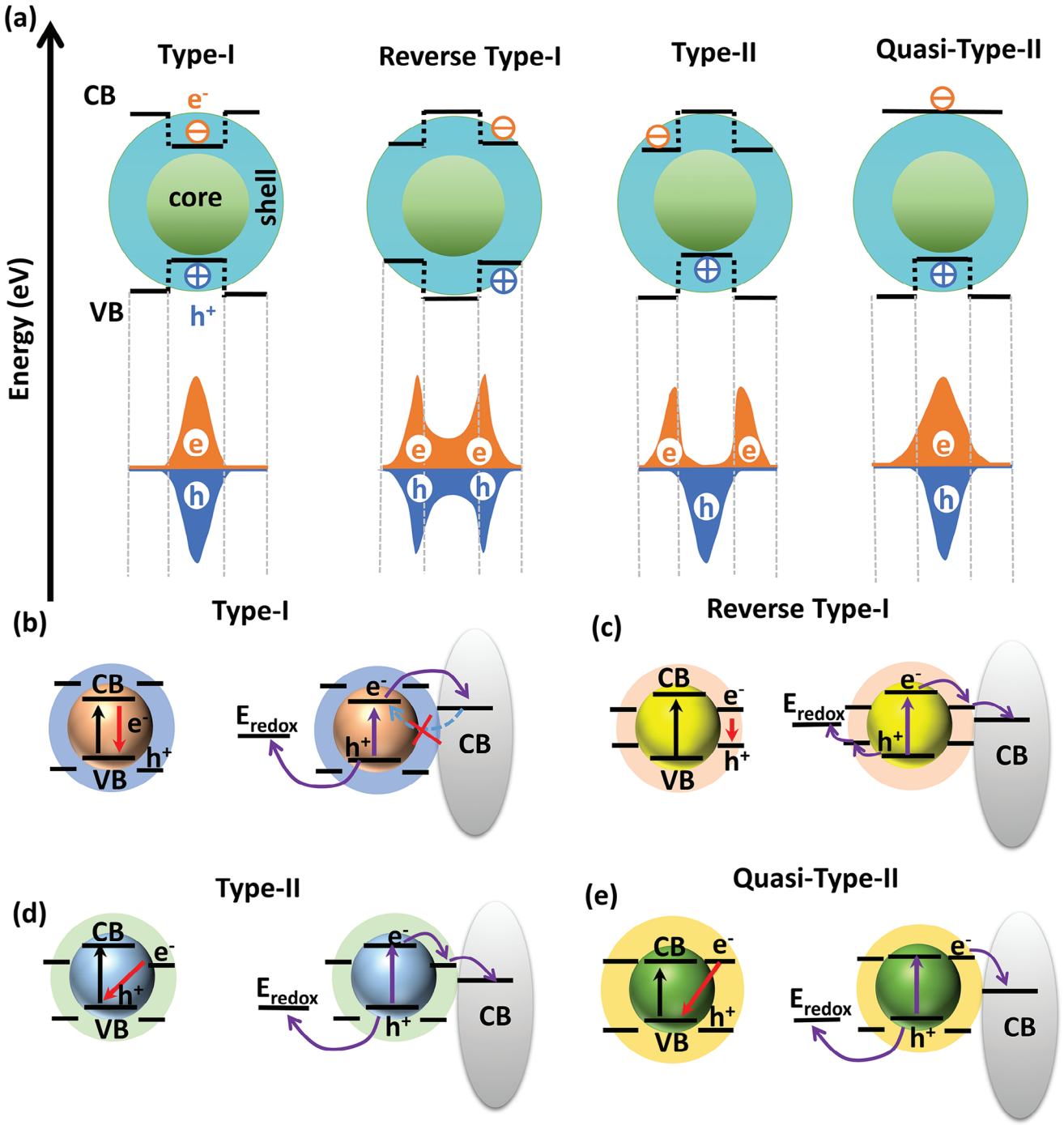

Figure 4. a) Schematic representation of the energy level alignment and electron (dark red) and hole wave functions (grey) in different types of core/shell QDs. The main emissive charge recombination (left) and charge transfer processes from a different type of core/shell QDs to host semiconductors (right, using electron acceptor as an example) in b) Type-I, c) Reverse Type-I, d) Type-II, e) Quasi-Type-II core/shell QDs.

precisely controlling the core size and shell thickness.[106a] When this energy offset is small enough, only electrons (or holes) can be confined, while holes (or electrons) are partially delocalized in the entire core/shell structure. This type is called Quasi-Type-II (Figure 4e), such as $CuInSe_2/CuInS_2$ QDs.[48] Compared to Type-II, Quasi-Type-II QDs typically present better PLQY (≈40–50%) and stability[107] due to better electron (or hole) confinement in the core region.[106a,107] The decrease in spatial overlap between electron and hole wave functions leads to a reduced charge recombination probability and a prolonged PL lifetime[108] compared with Type-I and Reverse Type-I QDs. However, the electrons in Quasi-Type-II QDs can be captured by the defects of the

shell surface, resulting in a lower PLQY (40-50%)[109] than Type-I (60-90%).[110]

More importantly, the electronic band structures of core/shell QDs can be fine-tuned by adjusting the core size and shell thickness,[53,72,109a,111] which is due to changes in the core/shell QDs' effective bandgap and carrier localization through quantum confinement.[106a] For instance, in $CuInS_2$/ZnS, the positions of the CB and VB edges of $CuInS_2$ are −3.55 and −5.05 eV, and the ones of ZnS are −3.28 and −6.82 eV.[112] The small CB edge offset (0.27 eV) and large VB edge offset (1.77 eV) make it possible to tune $CuInS_2$/ZnS from Type-I to Quasi-Type-II by decreasing the core size or increasing the shell thickness, facilitating the electron transfer process.[112]

2.3. Tuning the Core-Shell Interface of QDs

The different lattice parameters of the core and shell materials induce a strain at the core/shell interface, causing the formation of structural defects.[113] The consequent interfacial traps may act as non-radiative recombination channels, reducing the PLQY and the charge transfer rate from QDs to charge acceptors. An effective strategy is to insert buffer layers with a lattice constant intermediate between the core and shell, forming core/intermediate shell/outer shell QDs (**Figure 5**). For instance, an interfacial oxide layer of phosphate in InP/ZnS was shown to play a crucial role in mitigating the lattice mismatch band alignment between InP and ZnS, resulting in a higher PLQY (38%) compared to that of the oxide-free QDs (4%).[114] However, the interfacial oxide layer also had a detrimental influence on broadening the PL spectra, thereby decreasing the color purity of PL emission.[114] To address this drawback, ZnSe was developed as a buffer layer in InP/ZnS QDs,[115] effectively reducing the lattice mismatch from 7.7% between InP (lattice constant a = 5.869 Å) and ZnS (a = 5.405 Å) to 3.3% between InP and ZnSe (a = 5.667 Å).[115b] Nevertheless, ZnSe has a narrower bandgap than ZnS,[116] which could cause the delocalization of excitons over the entire core/shell QDs, consequently decreasing their stability of QDs. Moreover, the lattice mismatch of ZnSe and ZnS (≈4.5%[117]) typically limits the shell thickness to a few monolayers. In this context, an alloyed or graded interfacial layer ($ZnSe_xS_{1-x}$), whose chemical composition gradually changes from one material to another, was developed (e.g., InP/$ZnSe_xS_{1-x}$/ZnS).[118] The S-rich $ZnSe_xS_{1-x}$ has a wider bandgap to confine the charge carriers into the core (higher PLQY of 80%) while broadening the full width at half maximum (FWHM) up to 54 nm. Meanwhile, the Se-rich $ZnSe_xS_{1-x}$ shell exerted a more significant narrowing of FWHM (≈38 nm) albeit with a lower PLQY (44%), likely caused by the electron delocalization toward the shell region according to the PL decay measurements.[118] Likewise, a longer carrier lifetime, higher PLQY and narrower FWHM were observed by adding interfacial layers, including InAs/GaP/InZnP/ZnSe[119] and ZnSeTe/ZnSe/ZnSeS/ZnS QDs.[120]

In addition to PL emission, the sharp interface in core/shell structures may hinder charge dissociation and transport due to the confinement of charge carriers and the interfacial defects caused by lattice mismatch.[110] With the introduction of an alloyed interfacial layer, both electron and hole wavefunctions can achieve increased leakage into the shell region, which is helpful for electron/hole transfer from QDs to charge acceptors.[23] This concept was demonstrated with $CuInSe_2$/$CuInSe_xS_{1-x}$/$CuInS_2$ QDs,[23] where the alloyed layer contributed to the smallest charge transfer resistance among TiO_2/ZnS (8.8 kΩ), TiO_2/$CuInSe_2$ (5.7 kΩ), TiO_2/($CuInSe_2$/$CuInS_2$) (2.53 kΩ) and TiO_2/($CuInSe_2$/$CuInSe_xS_{1-x}$/$CuInS_2$) (0.87 kΩ).

2.4. Adjusting the Shape and Surface of QDs

The geometric shapes of QDs determine the presence of different facets around the QDs and the wave function distribution of electrons and holes, significantly influencing their electronic structures and optical properties.[121] By taking advantage of different crystal symmetry characteristics, shape-controlled syntheses have paved the way toward the growth of non-spherical nanocrystals (e.g., pyramidal, bipyramidal, tetrapodal, triangular, dot-in-plate, and dot-in-rod).[53,122] Typically, the geometry of QDs can be fine-tuned by adjusting the synthesis parameters (e.g., core crystalline structure, temperature, shell material, and ligands).[122,123] $AgInSe_2$ QDs can be spherical, pyramidal, or prismatic, depending on the reaction temperatures.[124] The directly synthesized $CuInSe_2$/ZnS and $CuInS_2$/ZnS QDs typically inherit the pyramidal structure of the core with the triangular projected shape (**Figure 6**a–c),[53] however, spherical $CuInSe_2$/$CuInS_2$ can be realized by template-assisted synthesis (Figure 6d).[48] ZnSe shell growth on InP resulted in pyramidal InP/ZnSe, while ZnS growth on the similar InP core induced the formation of spherical QDs, mainly due to the smaller lattice mismatch between InP and ZnSe (3.2%) compared to ZnS (7.7%) (Figure 6e–h).[125]

In QDs with spherical shapes, electrons and holes can be confined equally in all dimensions, while the wavefunction overlap of electrons and holes may result in significant charge recombination.[126] Especially in the spherical QDs with shell thickness > 1.5 nm, the shell significantly hinders the charge transfer.[72,111b,127] The consequent hole accumulation may subsequently lead to the surface recombination and degradation of QDs under illumination.[72,111b,127] In the non-spherical core-shell QDs, electron-hole wave functions present better spatial separation, increasing the probability of exciton extraction and prolonging the PL lifetime. E.g., the average lifetime of pyramidal-shaped $CuInSe_xS_{2-x}$/CdSeS/CdS QDs (≈2 µs)[128] is much longer compared to that of spherical CdSe/CdS QDs (≈40 ns), spherical $CuInSe_2$/$CuInS_2$ thick shell QDs (≈300 ns), and spherical PbS/CdS QDs (≈1 µs),[48,72,127] indicating the efficient spatial separation of photogenerated electrons and holes in the non-spherical structure.

On the other hand, the dangling bonds on QD surfaces may serve as dopants, creating deep band-tail states and resulting in electron trapping.[21a] Strong bonds between surface atoms and surface insulating ligands (e.g., organic molecules, polymers, metal-free inorganic ions, or molecular metal chalcogenide complex) can passivate such traps, improving the stability of QDs.[130] Surface ligands can also ensure solution processability, modulate the reactivity of the precursors,[131] improve control over the nucleation/growth rates,[132] and adjust the phase[133] of synthesized QDs (Figure 6i). Besides, the ability of different surfactants to bind to different facets of QDs at different strengths was devel-

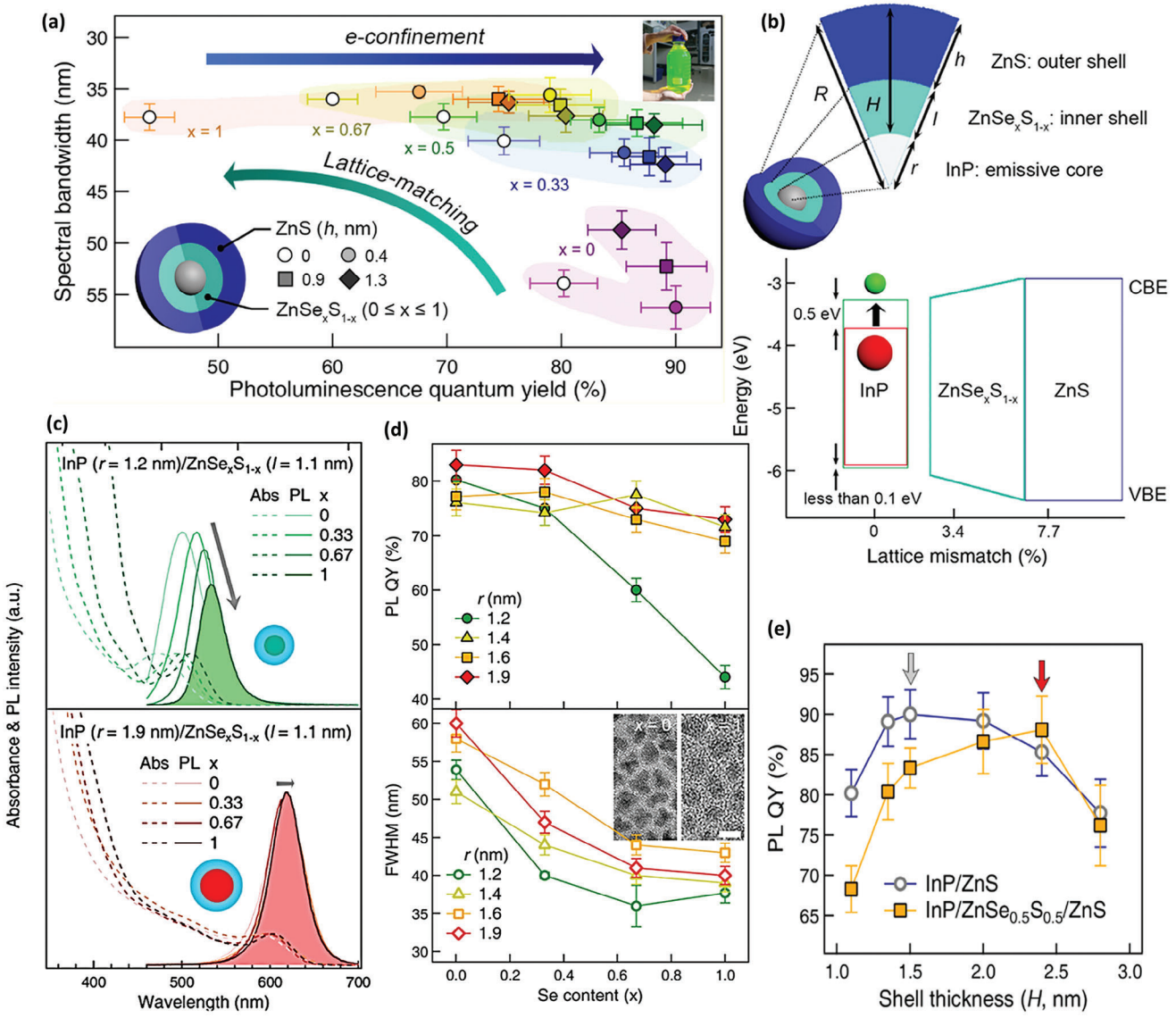

Figure 5. a) PLQY and FWHM of InP/$ZnSe_xS_{1-x}$/ZnS QDs with varying x and exterior shell thicknesses. Hollow circle, solid circle, square, and diamond refer to ZnS shell thickness h = 0, 0.4, 0.9, and 1.3 nm, respectively. b) Schematic illustration of InP/$ZnSe_xS_{1-x}$/ZnS QDs and the degree of lattice mismatch of shell materials from InP core. The CB edge of InP QDs shifts 0.5 eV as the radius (r) of InP decreases from 1.9 to 1.2 nm, whereas the VB edge energy moves less than 0.1 eV. c) Absorption (dashed line) and PL spectra (solid line) of InP (r = 1.2 nm)/$ZnSe_xS_{1-x}$ (l = 1.1 nm) QDs (top) and InP (r = 1.9 nm)/$ZnSe_xS_{1-x}$ (l = 1.1 nm) QDs (bottom) with different shell compositions (x = 0, 0.33, 0.67, and 1). d) Changes in PLQY (top) and FWHM of PL spectra (bottom) of different core-sized InP QDs (r = 1.2, 1.4, 1.6, and 1.9 nm) upon growth of $ZnSe_xS_{1-x}$ inner shell with different compositions (l = 1.1 nm, x = 0, 0.33, 0.67, and 1). e) Changes in PLQY of InP (r = 1.2 nm)/ZnS (navy open circle) and InP (r = 1.2 nm)/$ZnSe_{0.5}S_{0.5}$ (l = 1.1 nm)/ZnS QDs (orange square) as a function of the total thickness (H = l+h). (a–e) were reproduced with permission.[120] Copyright 2019, American Chemical Society.

oped to tune the morphology of QDs, using the fact that colloidal QDs aggregate to eliminate high-energy surface facets and minimize the overall surface energy.[134] At a proper temperature where stabilizing ligands are stripped off, facets with stronger binding affinity to ligands would become more reactive binding sites that accommodate growth species. For instance, by employing tris(dimethylamino) phosphine and indium trichloride, the In-rich (111) facets can be stabilized by co-passivation with halide and primary amine and grow slower, producing tetrahedrally-shaped InP instead of spherical shapes.[135] More importantly, ligands can also tune the band structure and consequent optical properties of QDs.[136] Jasieniak et al.[137] observed a marked effect of the surface ligands on the ionization energy. Later, Brown et al.[138] measured the energy shift of QDs treated with different ligands. The energy of the occupied and unoccupied surface states was pushed below the VB and the CB of the QDs, respectively. By combining experiments and ab initio simulations, Kroupa et al. pointed out that QDs' band-edge-energy shifts were

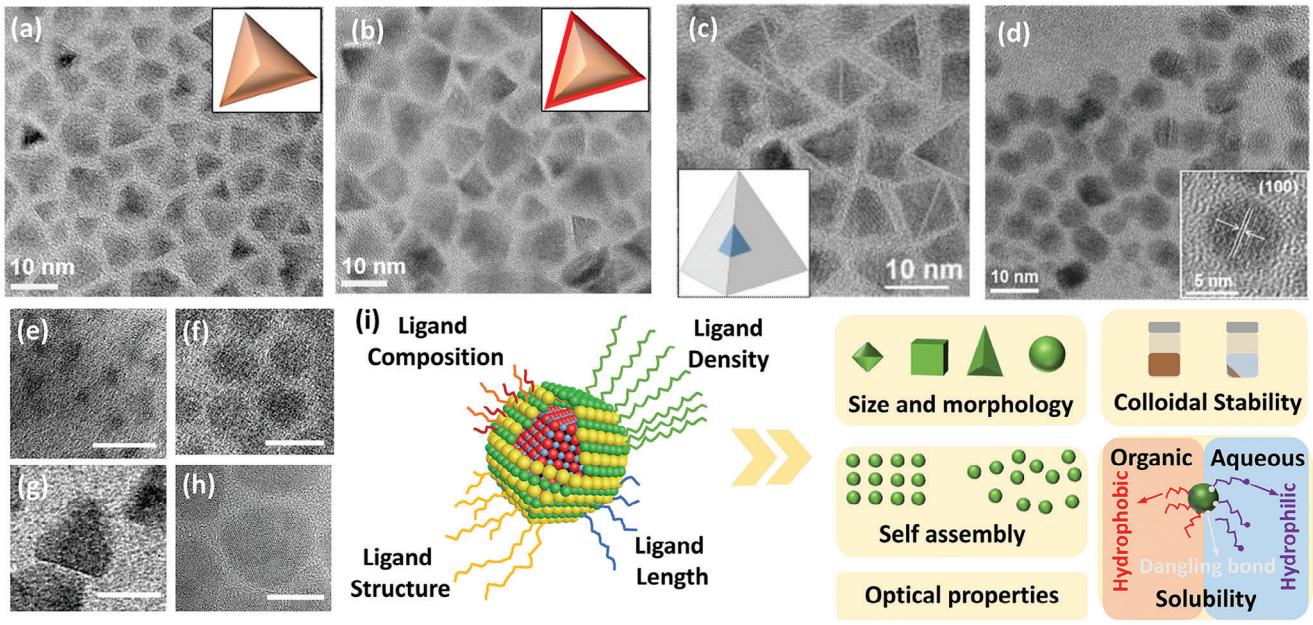

Figure 6. Transmission electron microscopy (TEM) images of a) CuInSeS QDs, b) CuInSeS/thin-ZnS QDs, c) $CuInS_2$/thick-ZnS QDs, d) $CuInSe_2/CuInS_2$ QDs, e) InP QDs, f) InP/ZnS QDs, g) InP/ZnSe QDs, h) InP/thick-ZnSe QDs, and i) InP/ZnSe/ZnS QDs. (a,b) were reproduced with permission.[53] Copyright 2016, Elsevier Ltd. (c) was reproduced with permission.[122a] Copyright 2017, American Chemical Society. (d) was reproduced with permission.[48] Copyright 2017, Wiley. (e,f) were reproduced with permission.[125] Copyright 2015, American Chemical Society. (h) was reproduced with permission.[129] Copyright 2017, American Chemical Society. i) The role of ligands in colloidal core/shell QDs.

proportional to the ligand dipole calculated in vacuum.[139] Moreover, ligand engineering allows the QDs' band structure to be adjusted by varying the composition and surface chemical state. For instance, ascorbic acid ligands were found to increase Zn content while decreasing In content, enlarging the bandgap of ZnCuInSe QDs and raising their CB level.[140] Besides, in PV and PC/PEC systems, the ligands link QDs to the supporting materials, potentially influencing charge extraction and transport. In most cases, the typical surfactant molecules consist of a long hydrocarbon tail and a polar head, such as oleylamine (OLA), oleic acid (OA), dodecanethiol (DDT), and trioctylphosphine oxide (TOPO). These ligands affect the surface trap states and act as insulating barriers for charge transport.[141] A practical solution to this issue is to partially or fully exchange the initial ligands of QDs with shorter-chain surfactants[141,142] or even single atoms.[143] For instance, by partially replacing OA with hexanoic acid (≈63% replacement), better charge injection can be obtained, achieving a maximum EQE of 21.4%.[17b] Sulfide ions (S^{2-}) "ligands" can endow InP/ZnS QDs with good water solubility and facilitate hole extraction from QDs to the surrounding acceptors.[25b] An ultrafast hole transfer (i.e., sub-picosecond) from QDs to a molecular acceptor (phenyldithiocarbamate, bound through hole-delocalizing ligands) was also observed.[144] This intriguing phenomenon can be explained by delocalizing the excitonic hole wave function into interfacial states formed by mixing PTC with the under-coordinated surface $^{+}$ sites of QDs.[145]

3. Synthesis of Heavy Metal-Free QDs

A range of wet chemical methodologies has been devised to synthesize colloidal QDs.[17e,27b,134,146] Here, we aim to concisely examine a crucial aspect relevant to solar energy applications: core/shell QDs. We conduct a comparative analysis of the merits and limitations associated with each method while also delineating recent advancements in this area.

3.1. Direct Synthetic Approach

3.1.1. Core Synthesis

Most core/shell QDs are synthesized through the initial synthesis of the core, followed by a final shell growth over the surface of the core. The ideal core should have a well-defined size, narrow size distribution, and a high degree of crystallinity. Proper surface ligand passivation is also needed to eliminate surface traps that may quench charge carriers.[147] The most representative direct synthesis of cores includes hot injection,[24,96,125,148] heating-up,[149] and solvothermal methods (**Figure 7a**).[150] The hot injection method, which involves a swift injection of reactive precursors into a vigorously stirred solution containing surfactant and a high-boiling point solvent, is beneficial to control the size and size distribution of QDs because it allows effective phase separation of rapid nucleation and growth stage.[24,96,125,148] However, this method relies on rapid and homogeneous reagents mixed at high temperatures for controlled nucleation. The mixing event becomes slower and less controllable with the increase in the batch volume. In the heat-up method, all reagents and surfactants/ligands are added to the same reaction vessel at a low temperature and heated to a high temperature at a controlled rate to activate the nucleation and growth of QDs.[149] The heat-up method provides a simple and reliable avenue for the scalable and

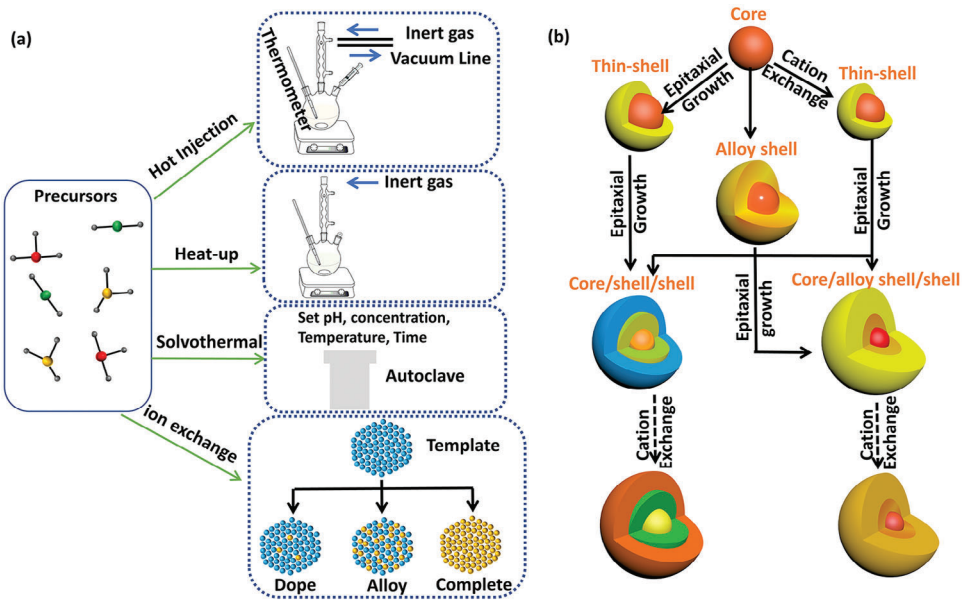

Figure 7. a) Representative methods to synthesize the core material. b) The typical routes for obtaining colloidal core/shell QDs.

reproducible synthesis of QDs. However, the synthesis of high-quality QDs using this method is limited in scope in terms of suitable ligands and precursors, requiring low reactivity of precursors below the desired temperature, rapid nucleation under the desired temperature, and appropriate decoupling of the nucleation and growth stages. Solvothermal synthesis operates in a liquid medium using organic solvents in a sealed pressure vessel. The closed system allows elevating the temperature above the solvent's boiling point, which increases the solvent's ability to dissolve the solid precursors, accelerates their reaction, and allows control over the shape, size, crystallinity, and size distribution of QDs. In addition, the solvothermal route does not require inert atmosphere or reflux conditions, making it easier to operate than hot injection and heat-up methods. However, this method also requires a relatively long time to increase the temperature to a target value, which results in difficult separation of the nucleation stage from the crystal growth stage, in turn making it difficult to achieve a uniform size and shape of the final product. The need for high-pressure equipment also makes it difficult to monitor the reaction process and investigate the growth mechanism. Finally, the high temperature and pressure create additional safety concerns, especially for large-scale synthesis.

For binary QDs, the synthesis challenges for III-V QDs include precursor selection and size control. For multinary QDs, it is challenging to obtain phase homogeneity, because the control over complex equilibria between multiple cation and anion precursors in a single reaction is hardly achievable.[17c] Alternatively, by incorporating the desired guest ions into the host binary or ternary QDs through partial ion exchange, alloyed ternary or quaternary QDs can be synthesized under highly controlled conditions without significant alteration of size and shape.[89b] For instance, $CuInS_2$ QDs synthesized by partial In^{3+} cation exchange with $Cu_{2-x}S$ adopt the hexagonal wurtzite structure[151] instead of the cubic chalcopyrite structure which is typically observed for $CuInS_2$ synthesized by direct routes.[152]

3.1.2. Shell Coating

To achieve high-quality core/shell QDs, the overcoating approach should allow the shell to grow with high crystallinity while avoiding the alloying and self-nucleation of the shell. Generally, shell coating can be achieved either through in situ epitaxial growth, cation exchange reactions, or a combination of cation exchange and epitaxial growth, depending on the thermal stability of the core materials (Figure 7b). In situ epitaxial growth allows the shell to grow by exposing the QD core to the precursors of shell elements while the core size and composition remain essentially constant. The wet colloidal one-pot synthesis, i.e., adding shell precursors right after core synthesis, was developed and applied to different QDs, including $CuGaS_2$/ZnS[24] and InP/ZnS.[153] Although this method is facile, it may be sensitive to unreacted precursors of the core (or side products) at the start of the shell growth. In such cases, an intermediate purification step, where the core undergoes precipitation/re-dispersion cycles, is required.[115a] Besides intermediate purification, other surface treatments may be needed before or during shell growth. E.g., hydrofluoric acid was employed in the early stages of shell growth to remove the accumulated oxidative defects of InP QDs.[17b–d] In particular, the growth temperature plays a crucial role in adjusting the shell growth rate[115b] and the crystal phase of the shell.[154] Generally, the reaction temperature should be high enough to provide energy equal to or greater than the reaction energy barriers required for shell growth.[155] However, when the in situ growth temperature of the shell materials is higher than the optimal temperature for core growth, the cores may experience unexpected Ostwald ripening (i.e., smaller QDs are broken down, and the dissolved species redeposit onto larger QDs, resulting in a broad size distribution[156]). Besides, the shell material may endure undesirable nucleation.[157] To deal with the above issues, the cation exchange approach (typically carried out <100 °C) was developed, where the shell is formed via a grad-

ual replacement of original cations in the core with newly introduced cations in solution.[110] The anion sublattice remains almost undisturbed, thus the shell grows at the expense of the core size. Examples include CuInSeS/ZnS,[53] CuInZnS/ZnS,[89b] and $AgInS_2$/ZnS,[95] where a PL blue-shift indicated the shrinking size of the core. By precisely controlling the composition of the reactant, the cation exchange method can realize the core/shell structures with various shapes and morphologies which are difficult or inaccessible to be prepared by direct syntheses, such as InP/GaP,[158] InZnP/InGaP,[159] $CuInSe_2/CuInZnS_{2-x}Se_x$,[160] and $AgInSe_2/AgInS_2$ QDs.[49] However, the shell grows at the expense of the core during cation exchange,[110] so the shell thickness is limited to the diameter of the starting QDs. It was found that the reaction does not proceed beyond a terminal shell thickness, even with larger excess cations for exchange and longer reaction times.[110] This issue can be alleviated by combining both cation exchange and epitaxial growth into the shell growth process,[122a] where a thin ZnS shell was first produced via cation exchange and thin-shell QDs were then made to react with Zn-precursor to grow a thicker ZnS epitaxially.

3.2. Indirect Template-Assisted Synthesis

Direct synthesis is challenging for complex-structured core/shell QDs. For instance, direct growth of $CuInS_2$ shell on $CuInSe_2$ QDs is difficult. The different reactivities of Cu and In precursors can induce mixed-phase intermediates (such as Cu_2S-In_2S_3[161]), making it difficult to control the shape and size of the final product. It was shown that adding the $CuInS_2$ precursor induced an island-like branched shell (not full passivation), and the excess precursors resulted in the formation of separate $CuInS_2$ QDs.[162] In this regard, template-assisted synthesis is a promising alternative.[48] For instance, CdSe/CdS core/shell nanorods[163] and octapods[164] have been employed as templates and were shown to undergo reversible cation exchange with Cu^+, producing $Cu_{2-x}Se/Cu_2S$ that inherit the structures of the CdSe/CdS templates. This elegant demonstration of the core/shell structure conservation was further developed,[165] where Cu_2Se/Cu_2S appeared as an intermediate during a sequential reaction from CdSe/CdS to ZnSe/ZnS. Quasi-Type-II colloidal $CuInSe_2/CuInS_2$ core/thick-shell QDs were synthesized by combining complete and partial cation exchange reactions.[48] The shape and shell thickness of QDs can be precisely controlled by tuning the initial QDs template.[23,48] However, specific unresolved issues persist. E.g., the surface ligands need to dynamically attach and detach to allow for the inflow and outflow of ions, while there is a lack of fundamental studies exploring the role of ligands in the ion exchange process within QDs. Additionally, the formation of lattice defects during the exchange and the retention of initial cations post-exchange remains poorly understood.

4. Solar Energy Conversion with Heavy Metal-Free QDs

4.1. Solar-Electrical Energy Conversion

QDs solar cells (QDSCs), which can convert solar energy into electrical energy via the PV effect, were first reported in 1998.[166] QDSCs include planar depleted-heterojunction QDSCs (record PCE of 18.1%[167]), QDs-polymer hybrid QDSCs (record PCE of 13.1%),[168] Schottky-junction QDSCs (record PCE of 9.92%),[169] and QD-sensitized solar cells (QDSSCs, record PCE of 16.38%).[60b] The most widespread heavy-metal-free core/shell QDSCs are QDSSCs (**Figure 8**a,b),[170] which consist of a conductive substrate, an electron transporting material (ETM), QDs, a redox-active electrolyte, and a counter electrode (CE). Upon solar radiation, the photogenerated electrons in the CB of QDs are quickly injected into the ETM and then into the CE via an external circuit. Simultaneously, the redox couple in the electrolyte captures the holes in the VB of QDs. The oxidized redox couple is reduced at CE by gaining electrons from the external circuit. However, undesirable charge recombination events may occur both within the QDs as well as at the host/QDs/electrolyte interfaces within a short time duration (from tens of picoseconds to hundreds of microseconds),[171] which release excess energy in the form of low-energy photons or waste heat, reducing the overall PV performance of QDSCs.[171,172]

To improve heavy-metal-free core/shell QDSCs, increasing efforts have been deployed to increase exciton generation, including facilitating charge separation/transfer and reducing charge recombination. Type-I core/thin-shell QDs were developed for QDSSCs because the thin shell can create an energy barrier at the ETM/QDs interface, reducing the charge recombination between the electrons in ETM and holes (or traps) in QDs.[173] For instance, Zn-doped Type-I $CuInS_2$/ZnS QDs were developed to sensitize ZnO nanowires for a QDSSC, whose PCE can be readily improved more than 2–3 times compared with the one without ZnS coating.[173a] However, the maximum PCE was limited to 0.71%, which could be partially attributed to the corrosive behavior of the I^-/I^{3-} electrolyte and the consequent high electron recombination at the QD/electrolyte.[172,173] To mitigate this issue, sulfide/polysulfide (S^{2-}/S_n^{2-}) was developed as an alternative electrolyte,[174] boosting the PCE of liquid junction $CuInS_2$/ZnS-based QDSSCs up to 7.04%.[173b] Besides, to ensure efficient QD deposition and charge transport, shorter mercaptopropionic acid (MPA) ligands were employed to replace OLA before loading $CuInS_2$/ZnS core/shell QDs into the TiO_2 film.[173b] However, surface traps may emerge during the ligand exchange. Improvements were made through a direct aqueous synthesis of water-soluble MPA-coated $CuInS_2$/ZnS core/shell QDs under ambient conditions, achieving an enhanced PCE of 8.15%.[175] Despite these advances, the energy barrier of the shell in Type-I QDs is not favored for electron injection from QDs to ETL. Considering this challenge, Liu et al. tuned $CuInS_2$/ZnS QDs from Type-I to Quasi-Type-II by suitably tuning the ZnS shell thickness, significantly improving the PCE of solar cells from 0.75% for one-monolayer ZnS shell to 2.07% for five-monolayer ZnS shell.[112] However, further increases in ZnS to ten monolayers led to a decline in device performance, possibly because the lattice mismatch between $CuInS_2$ core and thick ZnS shell (2.2%) may increase the interfacial defect density for thicker shells.[173a] In this regard, ZnSe was developed as shell material with a lower CB edge than ZnS and a smaller lattice mismatch with ZnCuInSe core and TiO_2.[59] Another significant obstacle limiting the performance of QDSSCs is the low QDs loading. Zhong's group introduced a secondary QDs deposition approach that creates new adsorption sites by forming a metal oxyhydroxide layer (via

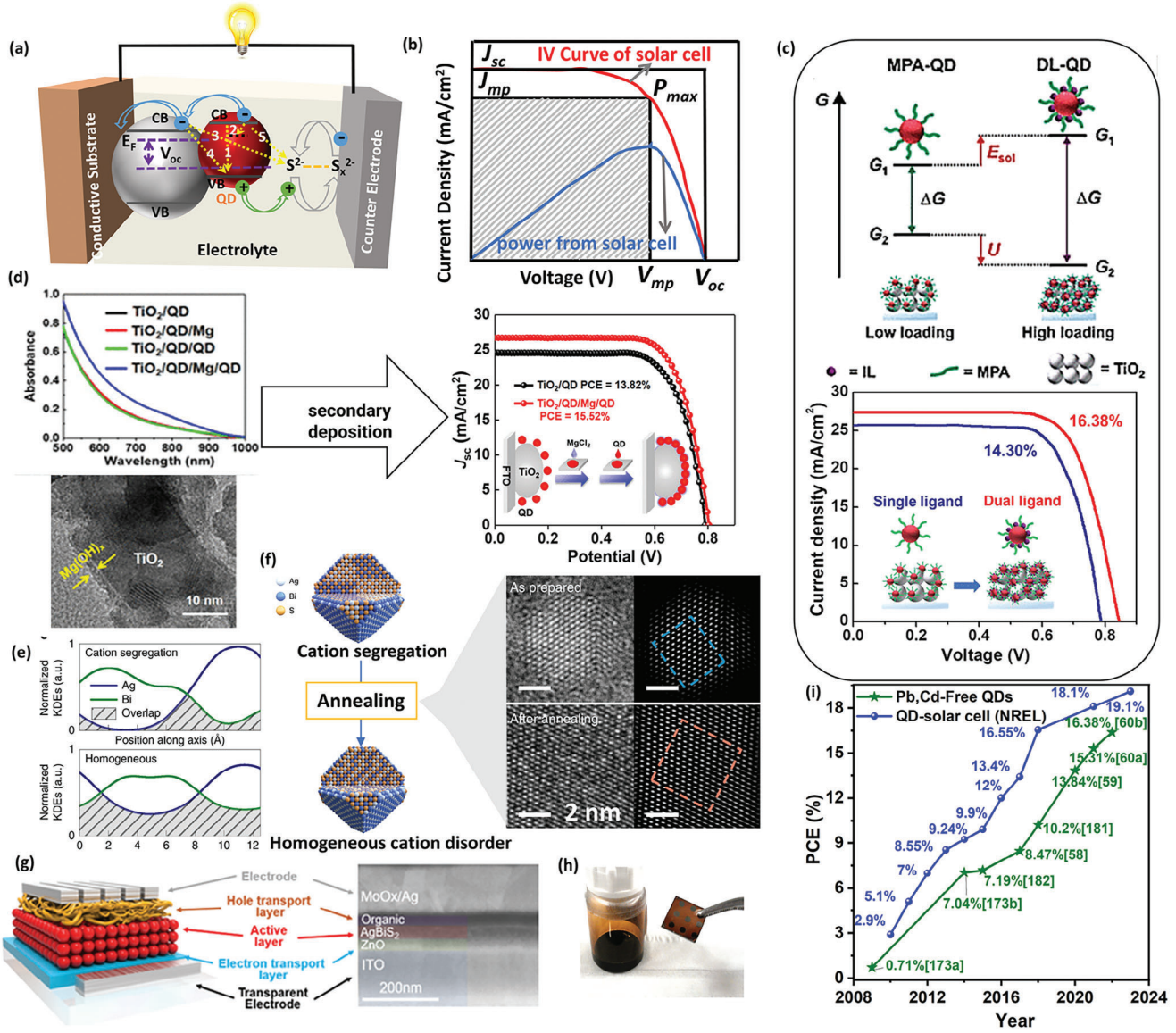

Figure 8. a) Schematic illustration of liquid-junction QDSSCs. Numbers refer to the undesired charge recombination processes 1) within the QDs; (2) at surface defect/trap states; (3) between photoinjected electrons in the CB of the ETM and the electrolyte; (4) by back transfer of electrons from the CB of ETM to the VB of QDs; (5) between the photoexcited electrons in the CB of QDs and the electrolyte. b) *J-V* characteristic curves of QDSCs. The PV performance is commonly characterized by P_{max}: the peak power; V_{oc}: the open-circuit voltage; J_{sc}: the short-circuit current density; and FF: the fill factor. The overall PCE of solar cells is defined as $\eta_{PV} = (J_{SC} \cdot V_{OC} \cdot FF)/P_0$, where *Jsc* is the short-circuit current density and P_0 is the integrated solar power density in $Wm^{-2}nm^{-1}$, i.e., AM 1.5G as the standard input. c) Variation of Gibbs free energy (G) and J-V curves of QDs in loading process based on MPA- and Dual Ligand-capped QDs. Reproduced with permission.[60b] Copyright 2022, American Chemical Society. d) UV–vis absorption spectra, TEM image and J-V for TiO_2/QD/Mg film electrodes. Reproduced with permission.[60a] Copyright 2021, American Chemical Society. e) Normalized kernel density estimates (KDEs) of Ag and Bi, f) schematic and HRTEM images of $AgBiS_2$ NCs with cation segregation and homogeneous cation disorder after annealing at 200 °C. (e,f) were reproduced with permission.[41d] Copyright 2022, The Authors. g) Schematic and cross-section image of the $AgBiS_2$ QDSCs. Reproduced with permission.[41c] Copyright 2024, Wiley. h) Photograph of $AgBiS_2$ solution and thin-film solar cell. Reproduced with permission.[41e] Copyright 2016, Macmillan Publishers. i) The record PCE values of QDSCs [data source: National Renewable Energy Laboratory (NREL)[167]] and liquid-junction QDSSCs are based on heavy-metal-free core/shell QDs. All values were tested under one sun illumination (100 mW cm^{-2}, AM 1.5 G).

$MgCl_2$ treatment) around QD-photoanodes (Figure 8c).[60a] They proposed using dual MPA and inorganic ligands to reduce solvation energy, thus facilitating QD loading (Figure 8d).[60b] These dual ligands also act as effective cross-linkers, reducing interdot repulsion and enabling the formation of dense QD layers, thereby achieving a champion PCE of 16.38% for QDSSCs.[60b]

Compared to liquid-junction solar cells, thin-film PVs eliminate the need for liquid electrolytes, offering advantages such as lightweight construction, reduced material consumption, and flexibility in design. The thinner absorber layers can enhance charge carrier collection and minimize charge recombination. Moreover, these PVs enable efficient absorption in small vol-

Table 2. Comparison of various heavy-metal-free different types of QD-based solar cells.

Type of QDs	Solar Cells Configuration	ETL	HTL	J_{sc} [mA/cm^2]	V_{oc} [V]	*FF* [%]	PCE [%]	Ref.
Ag_2S	Liquid junction	TiO_2	Polysulfide	7.26	0.33	40.8	0.98	[29]
Ag_2Se	Liquid junction	TiO_2	I^-/I_3^-	28.5	0.27	23.8	1.76	[30]
ZnCuInSSe	Liquid junction	TiO_2	S^{2-}/S_n^{2-}	26.52	0.802	72	15.31	[60a]
ZnCuInSSe	Liquid junction	TiO_2	S^{2-}/S_n^{2-}	26.99	0.838	72.4	16.38	[60b]
Ag_2S/ZnS	Liquid junction	TiO_2	S^{2-}/S_n^{2-}	5.12	0.23	43	0.5	[33]
$AgInSe_2$/ZnS	Liquid junction	TiO_2	S^{2-}/S_n^{2-}	14.54	0.644	55.9	5.23	[45]
$AgInS_2$/ZnS	Liquid junction	TiO_2	S^{2-}/S_n^{2-}	6.78	0.471	57	1.83	[178]
$AgInS_2$/ZnS	Liquid junction	TiO_2	S^{2-}/S_n^{2-}	8.34	0.49	55	2.25	[44]
$CuInSe_2$/ZnS	Liquid junction	TiO_2	S^{2-}/S_n^{2-}	22.61	0.583	52	6.79	[47]
$CuInS_2$/ZnS	Liquid junction	ZnO	I^-/I^{3-}	3.21	0.445	49	0.71	[173a]
$CuInS_2$/ZnS	Liquid junction	TiO_2	S^{2-}/S_n^{2-}	9.12	0.51	45	2.07	[112]
$CuInS_2$/ZnS	Liquid junction	TiO_2	S^{2-}/S_n^{2-}	20.65	0.586	58	7.04	[173b]
$CuInS_2$/ZnS	Liquid junction	TiO_2	S^{2-}/S_n^{2-}	9.6	0.6	42	2.42	[175]
ZnCuInS/ZnS	Liquid junction	TiO_2	S^{2-}/S_n^{2}	22.62	0.613	61	8.47	[58]
ZnCuInSe/ZnSe	Liquid junction	TiO_2	S^{2-}/S_n^{2-}	26.70	0.780	66	13.84	[59]
ZnAgInSe/AgInZnCdSe	Liquid junction	NiMo	S^{2-}/S_n^{2-}	19.06	0.49	52	4.71	[179]
(Al/Zn)-CuInSe/ZnSe	Liquid junction	TiO_2	S^{2-}/S_n^{2-}	27.34	0.632	60.9	10.61	[173c]
$AgBiS_2$	Solid QDSCs	ZnO	PTB7	22.1	0.45	63	6.31	[41e]
$AgBiS_2$	Solid QDSCs	ZnO	PBDB-T-2F	24.9	0.48	61	7.3	[41b]
$AgBiS_2$	Solid QDSCs	ZnO	BHJ	22.33	0.54	67.13	8.11	[41c]
$AgBiS_2$	Solid QDSCs	SnO_2	PTAA	27.1	0.495	68.4	9.17	[41d]
$AgBiS_2$	Solid QDSCs	ZnO	PBDB-T-2F:BTP-4Cl	27.07	0.494	68.1	9.1	[41a]
InP/ZnS	QD-organic cell	ZnO	MoO_3	18.4	0.798	69.3	10.2	[180]
$CuInS_2$/ZnS	QD-organic cell	TiO_2	MoO_3	14.45	0.87	57.52	7.19	[181]
InP/ZnS	QD-organic cell	SnO_2	PEDOT: PSS	25.48	0.845	70.63	15.22	[182]

umes, leading to a higher carrier density. In this context, ternary $AgBiS_2$ QDs have been developed for thin-film PVs, due to their favorable band gap range of 1–1.3 eV (allowing light absorption in NIR region), high extinction coefficient (≈10^5 cm^{-1}), and high stability under ambient environment.[41] Theoretical calculations indicate that $AgBiS_2$ thin-film PVs can achieve a high short circuit current of ≈22 mA cm^{-2} and a V_{oc} of ≈1 V, resulting in a PCE of 20%.[176] However, the actual V_{oc} of most $AgBiS_2$ thin-film PVs is ≈0.5 V and the fill factors of $AgBiS_2$ thin-film PVs are <70%. One possibility is the inhomogeneous cation disorder, and the consequent spatial separation of the Ag-derived VBM and Bi-derived CBM forms a cation-segregated configuration (Figure 8e). Through annealing at 200 °C, cation homogenization induced an enhanced optical absorption and better charge extraction, improving the V_{oc} and FF simultaneously (Figure 8f).[41d] Another direction is optimizing energy level structure by choosing a suitable hole-transporting polymer layer at a lower highest occupied molecular orbital level (Figure 8g,h).[41a] Besides, ligand passivation presents as an effective way to alleviate severe charge recombination losses, such as replacing ethanedithiol ligand with tetramethylammonium iodide,[41e] quadruple-ligand ensemble to realize multi-facet passivation,[41c] and using MPA to realize faster charge transfer and water solubility of QDs.[41b]

Table 2 summarizes progress in developing heavy-metal-free QDSCs. Figure 8i compares record PCE trends of QD solar cells (QDSC) (blue color) and liquid-junction QDSCs based on Pb, Cd-free QDs (green color). Despite significant advances, the record PCEs of 16.38%[60b] for QDSSCs remain below the theoretically predicted values (Schockley-Queisser limit of 33% for single-bandgap PV and over 40% for MEG-based QDSCs[5b]), mainly due to undesirable non-radiative carrier recombination processes within colloidal QDs and the slow carrier dynamics at the interfaces. Addressing these challenges requires the development of high-quality QDs characterized by a reduced density of surface trap states, a broad absorption spectrum with optimized electron band alignment, and stability in the surrounding environment. Furthermore, exploring the combination of different sensitization approaches, so-called co-sensitization[50b,51] or secondary deposition,[177] could further improve QDs loading and facilitate electron injection, hence increasing the J_{sc} of solar cells. Also, the well-known QDSCs trade-off between J_{sc} and V_{oc} can be minimized by optimizing other components, including the photoelectrode's structure and morphology, the electrolyte (or HTM) redox potential, and the CEs.

Heavy-metal-free QDs were also developed as a third component for polymer solar cells. For instance, the energy levels of $CuInS_2$/ZnS QDs align well with the PCDTBT polymer donor and PC71BM electron acceptor (**Figure 9a**), effectively enhancing the charge carrier generation.[181] The PL emission

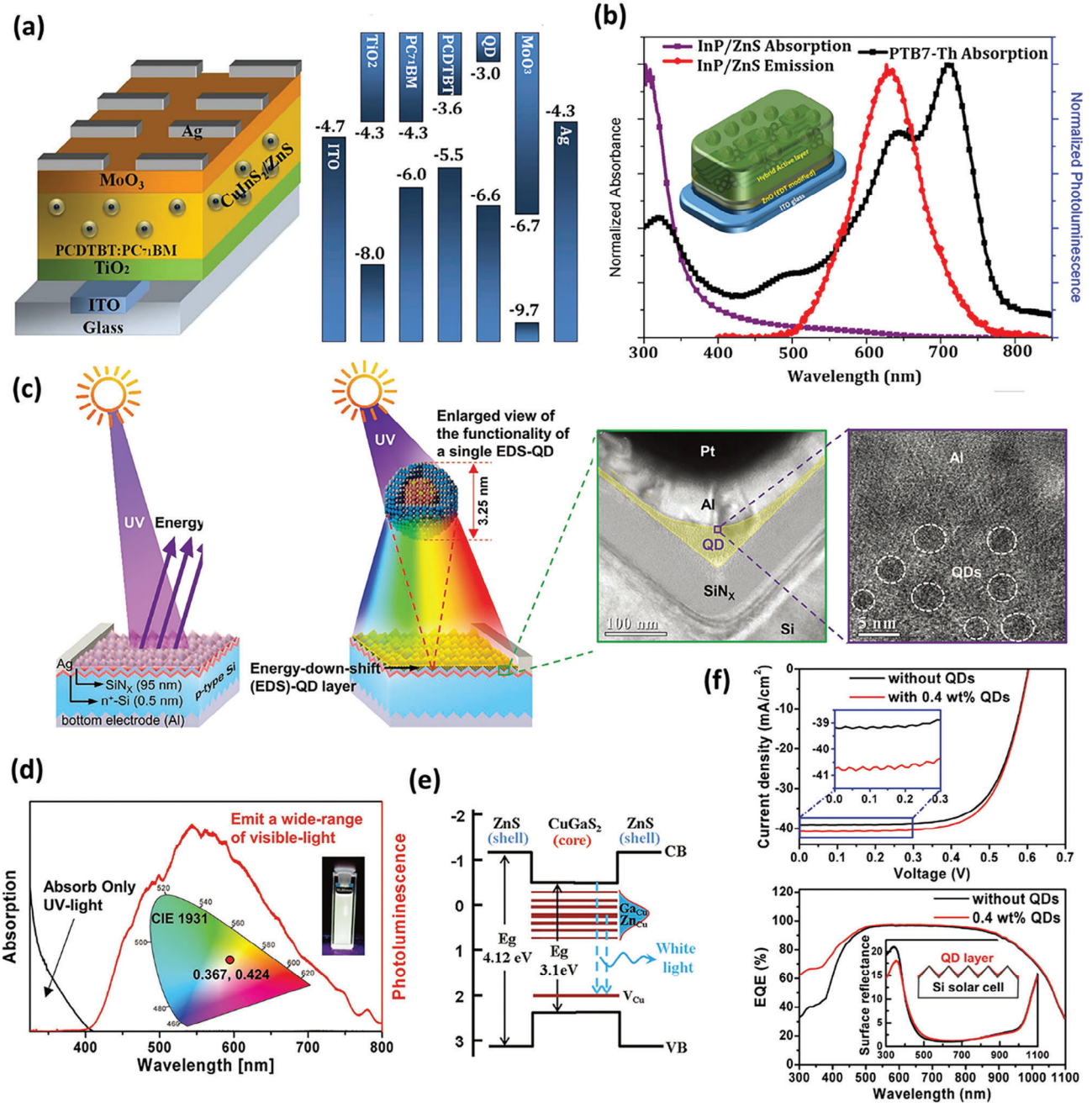

Figure 9. a) The structure diagram and energy levels of $CuInS_2$/ZnS QD-polymer solar cells (PCDTBT works as an electron donor, and PC71BM works as an electron acceptor. b) Optical characteristics of PTB7-Th (FRET acceptor) and InP/ZnS QDs. c) Scheme of energy losses in typical monocrystalline *p*-type Si solar cells without (left) and with (right) QD-EDS layer. d) Absorption and PL as well as e) energy-bandgap alignment diagram of $CuGaS_2$/ZnS QDs. f) J_{SC}, V_{OC}, *FF*, and PCE versus $CuGaS_2$/ZnS QDs concentration. (a) was reproduced with permission.[181] Copyright 2015, American Chemical Society. (b) was reproduced with permission.[180] Copyright 2018, Wiley. (c–f) was reproduced with permission.[24] Copyright 2018, Wiley.

of the InP/ZnS QDs (500–800 nm) overlaps with the absorption range of the PTB7-Th donor polymer (550–800 nm), and the energy transfer from the QDs to the polymer improves the photocurrent of the device (Figure 9b).[180] Besides, with its diversity of nanostructure and size and its tunable optical and electrical properties, it holds great promise in mitigating surface defects of ETL. For example, after passivation by depositing a thin InP/ZnS QDs layer, the root-mean-square roughness of SnO_2 film was reduced from 6.04 to 3.12 nm, achieving higher charge extraction and collection efficiency.[182]

Moreover, most PV cells suffer from low EQEs in the ultraviolet (UV < 400 nm) wavelength region.[183] The excess energy of the UV photon dissipates as heat, causing accelerated degradation of PV cells.[184] In this context, QDs were employed as

an energy-down-shift (EDS) layer to convert UV photons into visible light that can be absorbed efficiently by the PV cells (Figure 9c).[24,185] $CuGaS_2$/ZnS QD-EDS layers were employed on the surface of monocrystalline *p*-type Si solar cells (Figure 9c). The $CuGaS_2$/ZnS QD-EDS layer selectively absorbs only UV light (<407 nm) and emits visible light in the 400–800 nm range (Figure 9d–f), which overlaps with the light absorption range of the solar cell (≈400–900 nm), enhancing the saturated photocurrent density and PCE.[24]

4.2. Solar-Fuel Energy Conversion

Solar energy utilization depends on factors like geographical location, day/night cycles, and climatic conditions. This intermittency has prompted advancements in solar technologies to convert solar radiation into clean chemical fuels.[2] When illuminated by solar light, QDs can capture optical energy and store it within chemical bonds through photocatalytic reactions, including H_2 generation and CO_2 conversion. The photocatalytic reaction involves three key steps: a) light absorption and formation of photoexcited holes and electrons, b) the migration of these generated holes and electrons to the catalysts' surface, and c) the initiation of surface chemical reactions.

4.2.1. Solar-H_2 Evolution

Water photo(electro)catalysis[186] is a promising approach for realizing solar-to-H_2 (STH) conversion, a concept dating back to the pioneering work of Fujishima and Honda.[187] Harnessing the high energy content per mass (143 MJ kg^{-1}[188]) of H_2 makes the solar-H_2 conversion cost-effective and partly addresses the storage challenges associated with the diffuse and intermittent character of solar irradiation. In a simplified depiction of water photo(electro)catalysis, redox reactions are driven by the separation of electron-hole pairs generated through incident photons. The quest for high STH efficiency, long-term stability, and cost-effectiveness[188] has prompted significant research efforts toward designing suitable QDs,[23,48,189] including engineering the energy band structure to maximize the solar energy conversion rate,[48,65] adjusting the core/shell band structure to facilitate the charge carrier transfer kinetics[23,63] and engineering the surface of QDs to maximize charge transport while maintaining long-term stability.[25b,190]

Solar-driven H_2 generation from water can be broadly categorized as PC[191] and PEC processes.[192] PC reactions typically occur with powdered photocatalysts dispersed in an aqueous solution (**Figure 10**a,b). Typically, ligands of QDs significantly influence the PC reaction. The redox reactions cannot proceed unless the photogenerated charges tunnel through the ligand layer and move to the active sites. The conventional long-chain organic ligands (such as OA and OLA) inhibit the charge carrier transport behavior, increasing the non-radiative carrier recombination[141] and consequently hindering H_2 generation.[25b] In comparison, short-chain surfactants[141,142] and inorganic ligands (Cl^-, PO_4^{3-}, S^{2-})[143] can efficiently extract holes at the surface of QDs and simultaneously decrease the physical and electrical barriers for electron transfer from QDs to an electron acceptor, consequently facilitating charge separation and transport.[25b] Another strategy to promote charge transfer involves doping QDs with metal cations, where the dopant serves as charge trap sites to capture photoexcited holes effectively. For instance, Cu was doped inside the ZnS shell of InP/ZnS QDs (Figure 10c).[63] The holes were captured by the Cu dopant sites (Figure 10c–e), which are far from the electrons in the InP core, decreasing the electron-hole overlap integral and consequent charge recombination. Besides, the incorporation of cocatalysts can alleviate hole accumulation by changing the water oxidation reaction mechanism, lowering the reaction energy barrier and accelerating the charge transfer process at the photoanode/electrolyte interface.[52,190,193] PC is suitable for large-scale H_2 generation, while it requires separation of the produced O_2 and H_2 (explosive gas mixture) after the reaction.

Alternatively, PEC cells can generate products at different electrodes (Figure 10f,g). Besides, an external bias is typically employed in the PEC system to compensate for the potential deficiency, which can form a surface space charge layer, achieving efficient charge separation. The operation principle of PEC is akin to liquid-junction QDSSCs, yet with two redox systems: one reacts with the minority charge carriers at the surface of the photoelectrode and the other reacts with the majority charge carriers entering the CE. Most QD-PEC systems are based on core/shell QDs due to their better stability,[53] and tunable charge transfer behavior from QDs to electron/hole acceptors. Previous studies on QD-PEC systems are primarily focused on thin-shell QDs, including $AgInS_2$/ZnS,[189] $AgInSe_2$/ZnSe,[46] $CuAgIn_5S_8$/ZnS,[57] and CuInSSe/ZnS.[53] The stability improves with increased ZnS (or ZnSe) shell thickness, and the Type-I core/shell structure hinders the charge separation/transfer. To alleviate this issue, Mn[65,66] or Cu[68] was doped into the core, which artificially builds a smaller offset between the CB of the core and shell, achieving a prolonged exciton lifetime and a lower charge transfer resistance compared to the original QDs. On the other hand, for the thick ZnS (or ZnSe)-shell-based QDs, the light absorption of the QDs is limited to the visible and NIR region due to the dominant role of the wide-bandgap of the ZnS (ZnSe) shell. The shell material was then replaced with narrow-bandgap materials, including $CuInSe_2$/$CuInS_2$[48] and $AgInSe_2$/$AgInS_2$ QDs.[49] A gradient interfacial layer between the core and shell can further improve the PEC performance by alleviating the unwanted charge traps at the core/shell interface[23,49] Besides, co-catalysts can be employed to lower the kinetic barrier. For example, by decorating a $BiVO_4$-QD photoanode with $NiFeO_x$ (Figure 10h,j), both photocurrent density and stability were found to improve, probably because the co-catalysts can collect the photoinduced holes and act as a passivation layer to prevent photocorrosion of the photoelectrode.[194]

Table 3 summarizes the most recent advances in water photolysis based on various heavy-metal-free core/shell QDs. Despite considerable progress in the last decades,[195] the overall performance is still considered far from values suitable for commercialization (STH efficiency ≥10% and long-term stability ≥1000 h).[196] The solar energy conversion efficiency was still lower than that of toxic-metal-based QDs (such as PbS/CdS,[72,111a] CdSe/CdS[111b]), primarily due to insufficient charge generation arising from light-harvesting, undesirable

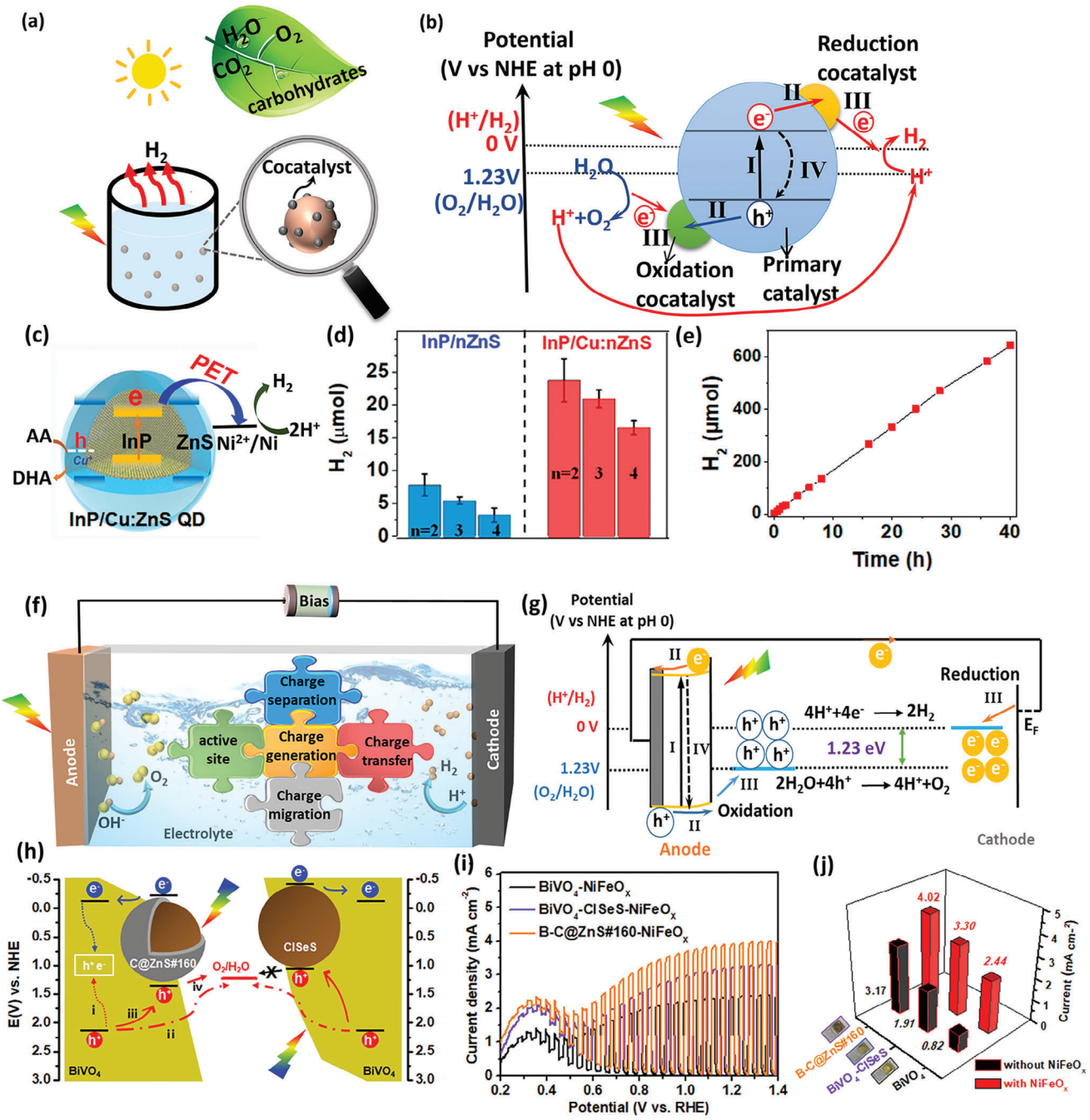

Figure 10. Schematic illustration of a) the configuration of a representative PC cell with powdered photocatalysts, which mimics photosynthetic organisms in nature, and b) energy diagrams of typical PC water splitting. c) Schematic illustration of PC H_2 generation based on the InP/Cu:ZnS QD photocatalyst, with Ni^{2+} as cocatalyst and ascorbic acid (AA) as sacrificial electron donor. AA is oxidized into dehydroascorbic acid (DHA) after the reaction. d) Comparison of the amount of H_2 of InP/nZnS (blue) and InP/Cu: nZnS (red) QDs with different ZnS shell thicknesses (n = 2, 3, and 4) under one h irradiation. e) Time course of the H_2 evolution reaction of InP/Cu:3ZnS QDs. f) Schematic illustration of a representative PEC cell configuration and g) energy diagrams (based on photoanode). h) Structure diagram of $BiVO_4$-CuInSeS/ZnS (B-C@ZnS#160) photoanodes with the $NiFeO_x$ co-catalyst for water oxidation. i) Comparison of photocurrent density of photoanodes deposited with the $NiFeO_x$ co-catalyst under chopped illumination. j) Comparison of the current density of all photoanodes under 1.23 V bias. (c–e) were reproduced with permission.[63] Copyright 2020, American Chemical Society. (h–j) was reproduced with permission.[194] Copyright 2021, American Chemical Society.

Table 3. Comparison of various heavy-metal-free QD-based water photolysis.

QDs	Abs edge [nm]	App	Reaction solution	Current density [mA/cm^2]	Product evolution rate	Stability[a)]	FE[b)]	Ref.
InP/ZnS	650	PC	H_2A	0.06	45 mmol h^{-1} g^{-1}	64.5 h	–	[25b]
Cu:InP/ZnS	600	PC	ascorbic acid	–	15 μmol h^{-1}	40 h	–	[63]
$CuInS_2$/ZnS	650	PC	NaHA/H_2A	–	1.59 mmol g^{-1}	70 h	–	[190]
$CuInS_2$/ZnS	650	PC	NaHA/H_2A	–	134 μmol	8 h	–	[193]
$Ag_xIn_xZn_{2(1-x)}S_2$	625	PC	H_2A	–	600 μmol	12 h	–	[52]
InP/Gap/ZnSe	650	PEC	NaOH	4.1	59.4 μmol cm^{-2} h	–	–	[37]
Zn-$CuInS_2$	780	PEC	ascorbic acid	0.15	50.4 mmol g^{-1} h	–	–	[38]
Zn-$CuInS_2$	780	PEC	PBB	3.8	–	–	91	[199]
SnSe/ZnSe	750	PEC	Na_2SO_3/Na_2S	7	60 mL cm^{-2}/day	85%	95	[36]
Cu-InP/ZnSe	650	PEC	Na_2SO_3/Na_2S	7.4	90.8 μmol cm^{-2}/h	89%	78	[34]
$AgInS_2$/ZnS	650	PEC	Na_2SO_3/Na_2S	5.7	32.5 μmol/h	62%	61	[189]
$AgInSe_2$/ZnSe	750	PEC	Na_2SO_3/Na_2S	7.5	48 μmol cm^{-2}/h	60%	–	[46]
Mn:$AgInS_2$/Cu:ZnS	630	PEC	Na_2SO_3/Na_2S	6.4	–	–	45	[67]
Cu:AgInSe/Cu:ZnSe	700	PEC	Na_2SO_3/Na_2S	8.5	88.1 μmol cm^{-2}/h		46	[68]
$CuAgIn_5S_8$/ZnS	650	PEC	Na_2SO_3/Na_2S	10.6	–	50%	–	[57]
CuInSSe/ZnS	1000	PEC	Na_2SO_3/Na_2S	5.3	–	70%	–	[53]
Mn:$CuInS_2$/ZnS	700	PEC	Na_2SO_3/Na_2S	5.7	7 μmol/h	75%	74	[65]
Mn:$CuInSe_2$/ZnSe	720	PEC	Na_2SO_3/Na_2S	6.0	–	67%	–	[66]
$CuInSe_2$/$CuInS_2$	1100	PEC	Na_2SO_3/Na_2S	3	–	80%	–	[48]
$CuInSe_2$/$CuInSe_xS_{1-x}$/$CuInS_2$	1100	PEC	Na_2SO_3/Na_2S	4.5	–	85%	80	[23]
$AgInSe_2$/AgInSeS/$AgInS_2$	1000	PEC	Na_2SO_3/Na_2S	1.1	–	–	50	[49]

[a)] For comparison, retention of photocurrent after 2 h (PEC) and time course of H_2 resolution (PC) are listed; [b)] Faradaic efficiency (%), the ratio between the experimental and theoretical estimated volume of H_2.

non-radiative carrier recombination within the QDs or at host semiconductors/QDs/electrolyte interfaces, and slow carrier injection/transfer rate from QDs to the electron/hole acceptors. Research efforts are still needed to control both the structure/composition of QDs and the configuration of PC/PEC systems to regulate the charge dynamics of the systems. Besides, UV-induced hole accumulation was reported as a reason for the self-oxidation of QDs.[197] An elegant solution to this problem can be developed by integrating PEC with LSCs,[198] where UV light is converted to visible light using QDs.

4.2.2. Solar-Driven CO_2 Reduction

Similar to the scenario in H_2 generation, colloidal QDs can be employed to reduce CO_2 under light irradiation.[32] Heavy-metal-free QDs including InP,[32] $AgInS_2$,[40] $CuInS_2$,[200] $ZnCuInS_2$,[201] $CuInS_2$/ZnS,[202] $CuAlS_2$/ZnS,[43] have been explored for CO_2 photoreduction. The selectivity and activity can be adjusted by suitably manipulating the defects in ternary QDs.[40,201] E.g., the density of copper vacancies can be varied to alter the distribution of optically active Cu^+ and Cu^{2+} defect states, and the Cu^{2+} defect states near the copper vacancy in $ZnCuInS_2$ QDs can effectively activate CO_2 to the COOH* intermediates (**Figure 11**a,b).[201] In addition, the combination of co-catalysts with QDs can significantly improve the photoreduction activity and selectivity (Figure 11c,d).[202] Nevertheless, it is essential to highlight that QD-based CO_2 photoreduction is preliminary. The efficiency and selectivity in the photocatalytic reduction of CO_2 using QDs remain relatively low, particularly concerning the production of usable fuels and value-added chemicals, specifically C^{2+} products. Currently, nearly all QD systems predominantly yield C1 products. Despite the higher value associated with C^{2+} products, achieving their photocatalytic generation poses a substantial challenge. Consequently, future research endeavors should prioritize exploring opportunities for selectively producing C^{2+} products, enhancing product selectivity, and deepening the understanding of the reaction mechanism involved in CO_2 reduction with QDs.

4.3. LSC

Despite significant advances in PV technologies,[167] the high cost of PV devices per unit surface area hinders their widespread adoption. Collecting solar radiation from larger areas and focusing ("concentrating") allows using smaller PV cells and can improve solar conversion efficiency. While the concentrated PV "solar plants" using motorized parabolic mirrors have been deployed on an industrial scale since 1982,[203] these require complex sun-tracking devices and do not work well with diffuse light (such as under cloudy weather). An alternative technology of LSC has been explored since the 1970s,[204] and has experienced rapid development since the ground-breaking work of Baldo and co-workers.[10,26b,205] Typically, an LSC consists of an optical waveguide (such as glass and polymer) embedded or coated with luminescent fluorophores (**Figure 12**a).[10,184,205c] The large surface area of LSCs harvests sunlight, penetrates through the matrix

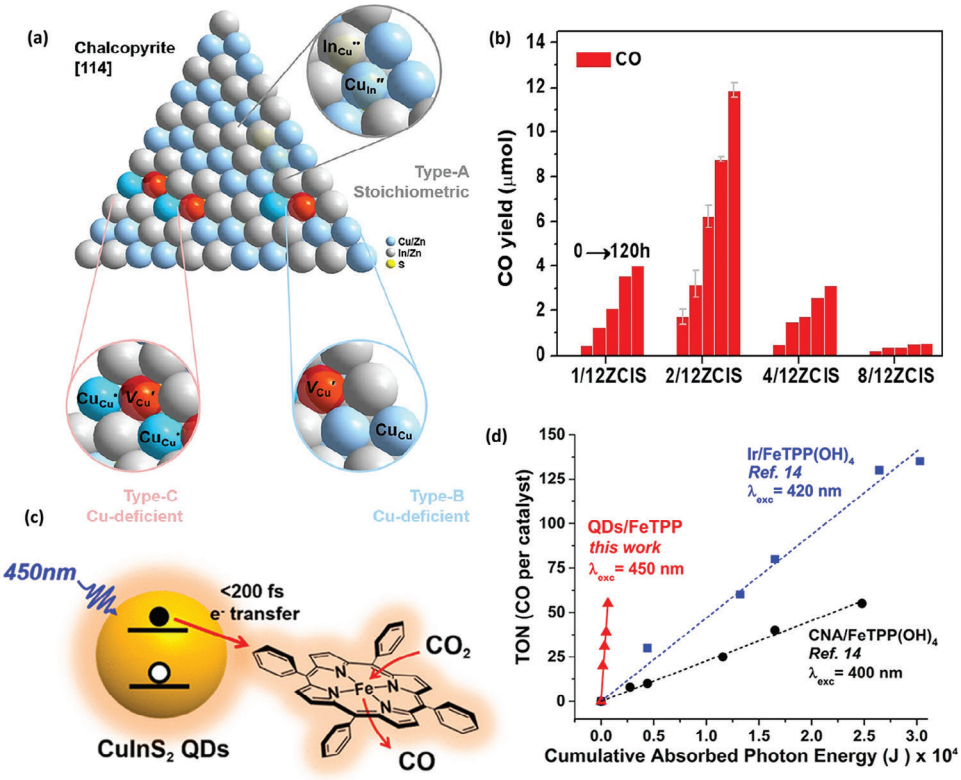

Figure 11. a) Manipulation of QDs' defect states and their effect on CO_2 adsorption. b) CO yield of the prepared QDs recorded every 24 h during 120 h solar simulator illumination ($380 < \lambda < 780$ nm, 100 mW cm^{-2}). c) Illustration of the use of electrostatic assemblies of negatively charged colloidal $CuInS_2$/ZnS QD sensitizers and meso-tetraphenyl porphyrin iron(III) chloride (FeTPP) to photo-reduce CO_2 to CO in water upon illumination with 450 nm light. d) Measurement of catalytic efficiency. (a,b) were reproduced with permission.[201] Copyright 2023, American Chemical Society. (c,d) were reproduced with permission.[202b] Copyright 2017, American Chemical Society.

and then gets absorbed by the luminophores. The luminophores re-emit the light as fluorescence or phosphorescence at a longer wavelength, which then undergoes multiple internal reflections from the LSC/air interface, being thus channeled to the narrow edges of the optical waveguide. Finally, the re-emitted photons are adsorbed by the PV device attached to the edge of the LSC and converted into electricity. By collecting solar energy over a large area (LSC top area), the flux of radiation incident onto the PV devices (LSC narrow edge) increases multifold compared to the direct collection using PVs with the identical area,[206] therefore significantly improving the power output of the PV devices and lowering the cost of produced electricity.[10,26b,184,205c] Additionally, downshifting the incident solar light to match the absorption profile of the PV material can further boost the PCE of PV cells.[184] Last, LSCs enable semi-transparent architectures by employing luminophores with specific absorption profiles/colors, making them attractive for building-integrated PV technologies (BIPVs, Figure 12b).[205b]

To achieve efficient LSCs by using QDs as fluorophores, the QDs should absorb sufficient incident radiation and efficiently produce down-converted luminescence. Reabsorption of light occurs if their absorption and emission spectrum overlap with each other; even a slight overlap can result in dramatic energy losses because the optical path along the emitted light propagation (LSC length) is several orders of magnitude higher than that of the solar light collection (LSC thickness, on the order of mm).[207] Core/shell QDs can fulfill the above requirements with tunable light absorption/emission spectra and high PLQY. In particular, their overlap in absorption/emission can be decreased using several strategies.[26b,35,107] Their absorption and emission overlap became smaller with the shell thickness increase (Figure 12c).[35] Besides, doping small amounts of metal ion impurities can effectively reduce the absorption/emission overlap of colloidal QDs.[77,208] For instance, in Mn-doped ZnSe/ZnS QD-LSCs,[85] the PL emission corresponds to the $^4T_1$-$^6A_1$ d-d transition (≈2.1 eV). At the same time, the absorption was dominated by the ZnSe host (Figure 12d), effectively removing any overlap between the absorption and emission spectra.[85] On the other hand, most QD-LSC present light absorption in the visible range (435–675 nm), thereby constraining the average visible transmittance (AVT, ≈50%) and the color rendering index (CRI) of transmitted solar light.[209] LSC panels' consequent strong color distortion can alter the chromatic perception from indoor to outdoor settings, leading to artificially induced color blindness.[17c] To achieve visible transparency, recent research focuses on QD-LSCs with a broad absorption range covering the entire UV–vis and NIR spectrum (100-800 nm, Figure 12e), such as NIR-active $CuInS_2$/ZnS[17c] and $AgInS_2$/ZnS QDs,[95] while these QDs typically result in limited AVT (40-50%) and brown coloring.[42] Alternatively, QDs that selectively absorb only

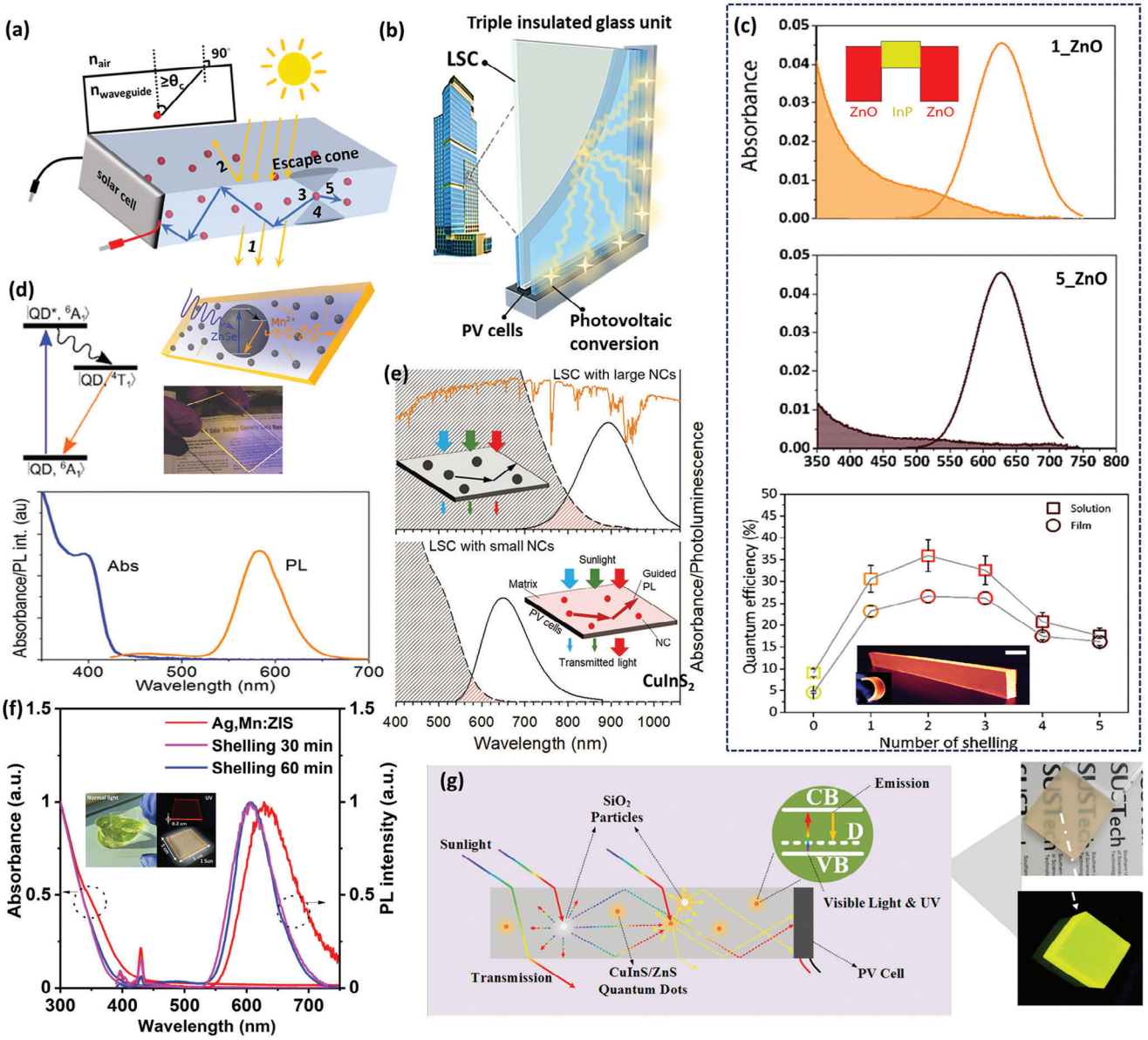

Figure 12. a) Schematic representation of LSC obtained by embedding QDs in a transparent polymer matrix. The numbers indicate the typical processes of energy loss in an LSC: [1] unabsorbed light; [2] light reflects from the top surface; [3] photon loss due to the non-unity of PLQY; [4] re-emitted light escape from the surface due to the angle smaller than the critical angle (the escape cone), and [5] light reabsorption by another QD. b) Illustration of LSC-based BIPV solar windows consisting of a triple-insulated glass unit embedding an LSC replacing the inner glass panel. c) Absorption (shading)/PL (no shading) overlap and LSC optical efficiencies of the InP/ZnO with different shell thicknesses. Inset: band alignment of InP/ZnO QDs. d) Schematic description of emission of Mn^{2+}: ZnSe/ZnS QDs and LSC. Bottom: absorbance and PL spectra of Mn^{2+}: ZnSe/ZnS QD-LSC device. e) Comparison between the normalized PL and optical absorption of $CuInS_2$ with radius a = 2.2 nm (top panel) and a = 1.0 nm (bottom panel). f) The normalized absorption and PL spectra of Ag,Mn:$ZnInS_2$ QD-LSC with different shell growth time. Inset: the photograph of Ag,Mn:$ZnInS_2$ QD-LSC. g) Schematic for $CuInS_2$/ZnS QDs-based LSCs with SiO_2 particles added to induce scattering effect. (c) was reproduced with permission.[35] Copyright 2018, American Chemical Society. (d) was reproduced with permission.[85] Copyright 2014, American Chemical Society. (e) was reproduced with permission.[215] Copyright 2019, WILEY-VCH. (f) was reproduced with permission.[75] Copyright 2024 The Authors. (g) was reproduced with permission.[214] Copyright 2018, Elsevier.

UV light (<400 nm) were employed for LSCs (Figure 12f),[75,210] while the limited light absorption of QDs restricts the PCE of LSCs. More complex shapes and compositions can overcome this restriction, including incorporating a resonant shifting bilayer cavity,[211] a distributed Bragg reflector,[212] and a photonic aperiodic mirror.[213] Two mirrors can be coupled to build an optical cavity to enhance the overall fraction of photons collected by the PV cells (Figure 12g),[206] while the lack of transparency hinders their application as BIPV. In this context, micron-sized SiO_2 particles were incorporated into QD-LSCs,[214] boosting the capture-ratio of sunlight through scattering the incident radiation.

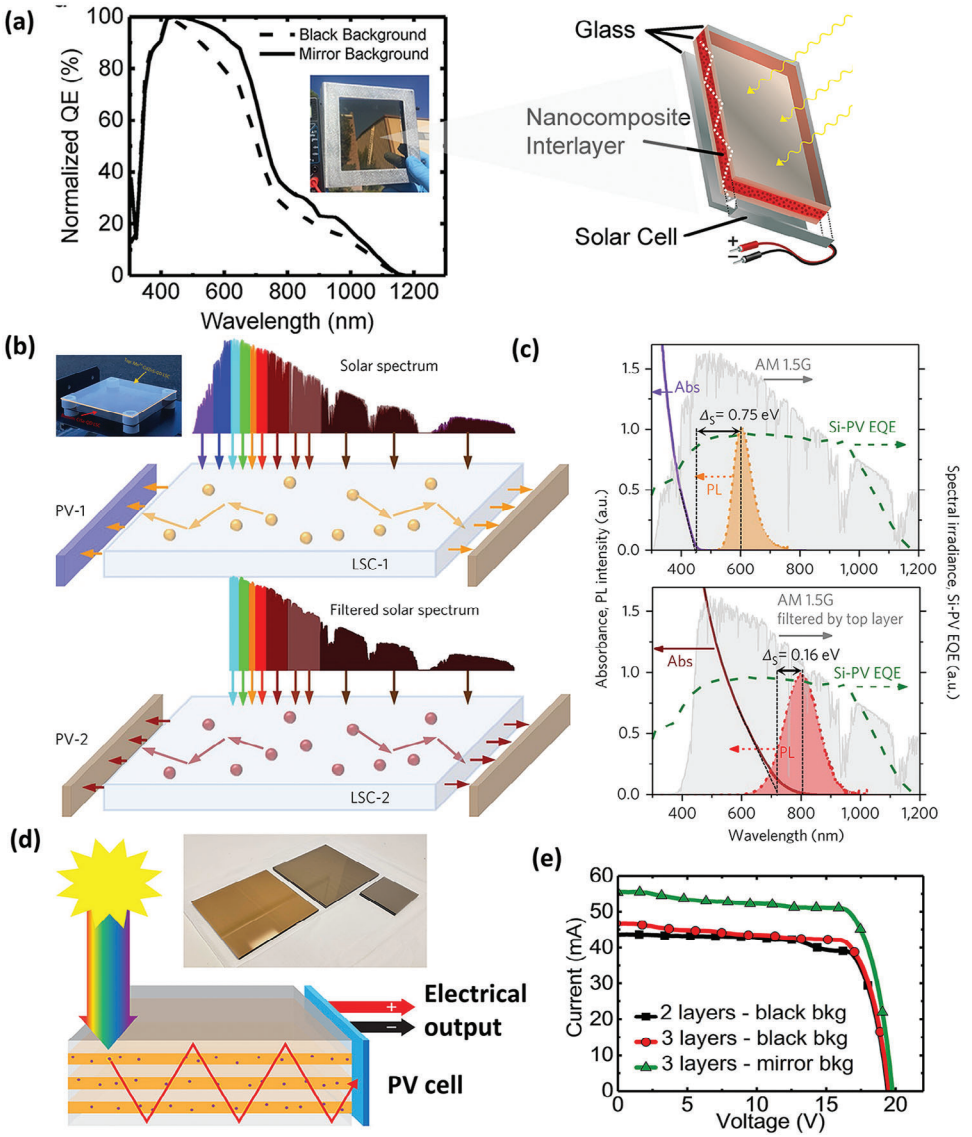

Figure 13. a) Diagram of the laminated-glass LSC design. Left: Absorption and PL spectra of colloidal $CuInS_2/ZnS$ QDs in toluene. b) Illustration of tandem LSCs, where a short-wavelength portion of the solar spectrum is absorbed by the first layer (LSC-1), and LSC-2 collects the longer-wavelength portion of the solar spectrum transmitted through LSC-1. Both layers are equipped with their own set of PVs. c) Absorption (purple) and PL (orange) spectra of Mn^{2+}-doped $Cd_xZn_{1-x}S/ZnS$ QDs used in LSC-1(up) and $CuInSe_2/ZnS$ QDs used in LSC-2 (bottom). The green dashed line refers to the EQE spectrum of a typical Si-PV; Grey shading refers to the AM 1.5G solar spectrum. d) Schematic illustration of a multi-interlayer LSC and e) corresponding I-V curves for two- and three-interlayer devices measured over a mirrored background. (a,b) were reproduced with permission.[42] Copyright 2018, American Chemical Society. (c,d) were reproduced with permission.[217b] Copyright 2018, Macmillan Publishers Limited, part of Springer Nature. (d,e) were reproduced with permission.[218] Copyright 2020, American Chemical Society.

On the other hand, besides the non-unity PLQY of QDs and reabsorption loss, a ≈25% energy loss arises from the top or bottom escape cone defined by Snell's Law assuming the waveguide refractive index n = 1.5 (the polymer: n = 1.3-1.5, glass: n = ≈1.5).[13,17c,107] To overcome the energy loss challenge and improve the stability of LSC simultaneously, a laminated LSC configuration was designed,[42] where the QD-polymer layer is sandwiched between two sheets of glass (**Figure 13a**). In this case, most of the waveguides and external surfaces are composed of glass, reducing the optical requirements for the polymer and eliminating the energy loss due to self-absorption and light escape. Alternatively, tandem LSC configurations were modeled[216] and experimentally developed.[205a,210,217] Generally, there are two or three layers in the tandem-structured LSCs (Figure 13b,c). This tandem configuration enhances light absorption efficiency by utilizing different layers to capture distinct segments of the solar spectrum, simultaneously addressing energy loss issues related to escape cones.[217] However, the tandem configurations require an air gap between the multiple LSC layers to avoid optical coupling. Additionally, incorporating separate sets of PV devices along the edges increases installation costs and complexity compared to single-layer LSCs. In this regard, the concept of

Table 4. Comparison of various heavy-metal-free QD-LSCs.

QDs	QY [%]	Abs Edge [nm]	PL range [nm]	Stokes shift [meV]	LSC size [cm]^3	η_{int} [a] [%]	η_{ext} [b] [%]	PCE [c] [%]	G [d]	Ref.
InP/ZnO	36	550	550–700	–	9 × 1.5 × 0.3	–	1.45	–	5	[35]
InP/ZnS	61	600	450–992	–	6 × 6 × 0.2	22.2	1.68	–	–	[221]
Cu:InP/ZnSe	87	650	650–900	650	10 × 10	37	–	–	–	[62]
$CuInSe_2S_{2-x}$ /ZnS	40	900	800–1250	530	12 × 12 × 0.3	–	3.27	–	–	[17c]
Laminated $CuInS_2$/ZnS	91	830	620–1240	>550	10 × 10	–	8.1	2.2	–	[42]
$CuInS_2$/ZnS	81	500	450–750	>85	2.2 × 2.2 × 0.3	26.5	–	1.8	7.3	[222]
$CuInS_2$/ZnS	65	500	450–700	–	2 × 2 × 0.8	–	–	1.68	2.5	[214]
$CuInS_2/ZnSe_xS_{1-x}$	70	600	440–800	–	10 × 10	–	0.53	–	–	[223]
CuGaAlS/ZnS	91	450	440–750	810	20 × 20 × 0.15	–	–	0.77	–	[55]
$AgInS_2$/ZnS	60	800	500–1240	–	5 × 5 × 3	–	3.94	–	1.6	[95]
$AgInS_2$/ZnS	64	600	500–900	–	10.4 × 10.4 × 0.2	27.4	3.8	–	13	[224]
Cu:ZnInSe/ZnS liquid	63	650	550–850	93	2 × 2 × 0.2	–	3.67	0.83	10	[64]
Cu:ZnInSe/ZnS polymer	63	650	550–850	93	2 × 2 × 0.2	–	1.75	0.83	10	[64]
Zn,Al:$CuInS_2$	–	800	600–900	–	1.8 × 1.8 × 0.1	–	6.97	–	4.1	[61]
Tandem $CuInSe_2$/ZnS	72	800	650–1000	–	15 × 15 × 0.16	–	6.4	1.8	2.2	[217b]
Tandem $CuGaInS_2$/ZnS	94.6	400	420–750	–	5 × 5 × 0.5	–	9.94	–	10	[56]
multiple-interlayer $CuInS_2$/ZnS	–	700	650–950	–	15.2 × 15.2	16	8	3.6	–	[218]

[a] η_{ext}, the external optical conversion efficiency, a ratio of output power from the LSC edges and the input power on the LSC top surface area exposed to light, also called overall optical efficiency, which can be experimentally measured by comparing the short-circuit photocurrent of a PV cell coupled to the LSC edges (I_{LSC}) and that of the same PV device illuminated directly in normal incidence (I_{PV}) with an identical light source;[219,225] [b] η_{int}, the internal optical conversion efficiency is a ratio of the number of photons emitted from the panel edges to the total number of absorbed photons, which can provide comparative information on the efficiency of photo transmission. It can be calculated by normalizing the η_{ext} with the absorption efficiency (the ratio of the number of photons absorbed by the LSC luminophore photons and the number of incident photons);[14] [c] PCE is defined as the ratio of output electric power of PV coupled with LSC and the input power;[226] [d] G refers to the geometric gain factor, which is defined as the ratio of the top area of the LSC exposed to solar light and the area of PV cells attached to the LSC edges.

"multi-interlayer" was combined with "laminated structure," and a three-interlayer LSC device composed of a laminated-glass configuration was recently developed (Figure 13d,e).[218] The main drawback of this architecture is that it requires a complex fabrication process.

In summary, the availability of Stokes-shift-engineered core/shell QDs boosted the development of QD-based LSCs. Despite promising progress (**Table 4**), achieving efficient large-area LSCs remains a challenge due to losses caused by reabsorption. Future research efforts should focus on optimizing the PLQY, the fraction of absorbed solar spectrum, Stokes shift, and stability of QDs through meticulous material selection and precise control of core, shell, core-shell interface, QD surface, etc. Developing new LSC architectures and waveguide materials is crucial to minimize energy losses attributed to the light "escape cone". Additionally, replacing conventional silicon cells with devices that match the PL of LSCs can enhance overall efficiency. Notably, most reported optical efficiencies are based on comparing short-circuit current density values with and without the LSC (where $G = Area_{LSC}/Area_{PV}$). However, this equation assumes that EQE_{PV} and EQE_{LSC} are constant and the same for all wavelengths.[219] Under broad-spectrum illumination, this may lead to significant errors when comparing the LSC of different absorption/emission profiles. To better compare various LSC systems, it is highly recommended to report the EQE_{PV}, EQE_{LSC}, and the overall PCE of LSC ($\eta_{PCE} = (J_{LSC-PV} \cdot V_{OC} \cdot FF)/P_0$).[219,220] The $J_{LSC\text{-}PV}$ is the short-circuit current density calculated by dividing the current by the waveguide front surface area because the front surface of the LSC is the area receiving the incident power.

5. Conclusions and Perspectives

In summary, we conducted a comprehensive review of cutting-edge research in the design and synthesis of environmentally friendly colloidal QDs used as building blocks in solar energy conversion, highlighting their tunable optoelectronic properties and charge carrier dynamics by engineering their composition, core size/shell thickness, core/shell interfacial layer, shapes and surface. We analyzed recent developments in QD-based solar energy technologies, including PV devices, solar-fuel conversion and LSCs. Despite considerable efforts to optimize synthetic approaches and enhance device performance, most heavy-metal-free core/shell QDs still fall short of the features exhibited by state-of-the-art Cd- or Pb-based QDs. This shortfall can be attributed to several factors: I) Synthesis challenges: Cd- and Pb-based QDs benefit from extensively researched and refined synthesis pathways that have been developed over many years. II) Difference in material structures and properties. Heavy-metal-free QDs possess distinct material structures and properties compared to Cd- or Pb-based QDs. For example, CdSe QDs typically exhibit a direct bandgap, whereas $CuInS_2$ QDs may have an indirect bandgap. This variation significantly impacts light absorption, emission efficiency, and charge carrier dynamics within the QDs, thereby influencing overall device performance. III) Device integration. Integrating QDs into practical solar devices involves

optimizing device architectures, interfaces, and processing techniques to maximize performance and stability. Cd- and Pb-based QDs have been integrated into various device structures, with well-established fabrication methods and performance metrics. Transitioning to heavy-metal-free QDs requires re-evaluating device designs and processing conditions to accommodate differences in material properties and device behavior. From our perspective, future research should prioritize the following directions:

5.1. Development of Innovative QD Synthesis

The intended applications of QDs require precise control of their optoelectronic properties. Therefore, the crystal structure, inner and surface defects, size, morphology, and composition of QDs should also be precisely controlled. Most current synthetic methods for colloidal heavy-metal-free QDs require high reaction temperatures (up to 320 °C) and toxic organic solvents/surfactants/precursors. Developing the synthesis of heavy-metal-free QDs at relatively low temperatures is an emerging direction. For instance, by utilizing S-OAm (S powder dissolved in OLA) as the sulfur source instead of DDT, $CuInS_2$/ZnS QDs can be synthesized at 130 °C, a departure from the conventional high synthesis temperature range of 200–240 °C.[227]

Additionally, the synthesis of QDs like InP/ZnSe and ZnSe/ZnS imposes stringent experimental requirements due to the pronounced vulnerability of precursors to moisture (e.g., Se-TOP). Alternative precursor materials and more efficient passivation strategies are needed. Facilitating interdisciplinary collaboration and knowledge exchange among researchers, industry stakeholders, and regulatory agencies could expedite the development and adoption of heavy metal-free QDs. Granting open access to data, resources, and best practices may stimulate innovation and promote responsible deployment of technology. Moreover, the integration of machine learning into the experimental process presents considerable potential for refining the selection of suitable precursors and ligands. By harnessing existing experimental data, machine learning algorithms can pinpoint critical parameters and provide guidance for exploration within the synthetic parameter space.[228]

5.2. In-depth Mechanistic Studies

After decades of research on QDs, the mechanistic details and the parameter space of their synthesis are still not well understood. Many studies have delved into the impact of various factors such as structure, core/shell interface, and surface on the QDs including InP, ZnSe, and ZnSeTe, while few focus on their charged and multi-exciton states, leaving the underlying physical and chemical mechanisms largely unexplored. Detailed insights are expected to be obtained from ultrafast spectroscopy technology and theoretical simulations. In addition, we anticipate scalable quantum computation through machine learning methods, which can automatically generate countless QD structures and predict their electronic properties.[229]

Furthermore, it is imperative to enhance our theoretical comprehension and conduct a thorough comparison of the electronic, optical, and defect characteristics between heavy-metal-based and heavy-metal-free QDs, which will lead to designing and optimizing heavy-metal-free QDs. For instance, theoretical understanding illustrates that the outstanding PV characteristics of lead halide perovskites stem from a blend of factors including the high symmetry perovskite structure, high electronic dimensionality, the presence of lone-pair Pb 6s, the inactive nature of Pb 6p, spin-orbit coupling (SOC) effects, the arrangement of polar organic cations, and the ionic properties of halides.[230] Therefore, to replace Pb, the candidate should possess lone-pair *s* orbitals and inactive *p* orbitals, which narrowed down the options to include In(I), Sb(III), Ge(II) and Sn(II) and Bi(III), *etc.*

5.3. Optimize Device Architectures

Heavy-metal-free QD-based solar devices face significant challenges related to environmental stability under ambient conditions. The solar conversion efficiencies of most devices are below the required targets for commercialization.

Multiple strategies could be explored to increase the efficiency of QD-based solar-electricity or solar-fuel conversion: I) developing new device architectures (e.g., "rainbow" architecture,[231] tandem structures,[111a,198] co-sensitization[50b,51] or secondary deposition,[177]) to improve light-harvesting. II) Engineering the band alignment between QDs and charge acceptors (e.g., mixed TiO_2 phases[232] and SnO_2-TiO_2 heterojunction[197]) and decorating well-designed cocatalysts to improve charge separation. III) Replacing surface ligands with shorter ones,[72] changing the morphology of charge acceptors (e.g., nanowire, nanotube, etc.), and combining low resistive guide materials [e.g., graphene nanoribbon networks,[233] graphenes,[234] and multi-wall carbon nanotubes,[235] to facilitate charge migration. IV) Engineering the QD-host interfaces to reduce charge recombination (introducing Al_2O_3 and ZnS surface passivation layers after QD-deposition). V) Optimizing other components, including better matching redox couples in the electrolyte and designing of CE with high electrical conductivity, high specific surface area, high catalytic activity, and chemical stability (such as Cu_2S CEs supported on carbon fibre paper substrate[236]).

Regarding QD-based LSCs, alternative LSC architectures and waveguide materials should be developed to decrease energy loss, such as coating the LSC with photonic crystals.[237] Tandem structures and plasmonic materials[238] can further enhance light absorption. Furthermore, conventional Si-cells can be replaced with cheaper and more scalable devices whose light absorption spectrum matches the PL of LSCs.[239]

5.4. Alternative Applications

In addition to the applications described above, the advantages and rapid development of heavy-metal-free QDs make them an ideal choice for addressing the challenges arising not only in sustainable energy technologies but also in biomedical applications, including in vivo biological imaging and detection[240] and theragnostic.[241] Heavy-metal-free QDs can also serve as an essential model material for exploring fundamental phenomena in both individual nanoparticles and their ensembles, including

analyzing the band-edge electronic states arising from long- and short-range exchange interactions and the particle shape effects on electronic energies within or near the quantum-confinement regime. In particular, alloyed and doped QDs allow testing the "wavefunction engineering" principle to control the spectral and dynamic behaviors of electronic excitations and carrier interactions.

5.5. Safety Assessment of Heavy-metal-free QDs

Besides, it is essential to evaluate the environmental and biological impacts of heavy-metal-free QDs by quantifying their toxicity and thoroughly analyzing their life cycles and environmental fate. The toxicity of QDs depends on several factors, including the physicochemical properties of QDs (such as size, charge, concentration, nature of the outer coating, and susceptibility to the oxidation, and photolysis), dosage, concentration etc.[242] Evaluating the toxicity or environmental friendliness of heavy-metal-free QDs is challenging and goes beyond simply examining the absence of specific toxic heavy-metal elements in QDs. For instance, it involves assessing the release of potentially harmful substances during synthesis, usage, and degradation. It also includes the impact of QDs on living organisms and ecosystems, considering bioaccumulation, biomagnification, and ecological disruption. Therefore, it is crucial to assess the overall effects of QD utilization on ecosystems, human health, and environment.[243] However, there remains a scarcity of comprehensive studies examining the toxicological aspects of colloidal QDs, with the majority of research in this area conducted by nanotechnology experts rather than toxicologists or health professionals. An upgraded toxicological research paradigm may help to better investigate the toxicity of QDs and build important steps in identifying a novel QD design and synthesis that is safe for human health and the environment.

In conclusion, leveraging substantial advancements in the development of synthesis and chemical processing techniques, alongside consistent endeavors to comprehend the optoelectronic characteristics and device efficacy of heavy-metal-free QDs, we anticipate these materials will swiftly evolve into pivotal constituents within various nascent solar technologies.

Supporting Information

Supporting Information is available from the Wiley Online Library or from the author.

Acknowledgements

F.R. and D.F.P. acknowledge support from individual Discovery Grants (Natural Science and Engineering Research Council of Canada (NSERC)), the Canada Foundation for Innovation (CFI) for infrastructure support and operating funds, and the Fonds de Recherche du Québec—Nature et technologies (FRQNT) for team grants. L. J. acknowledges the FRQNT for an individual Post-Doctoral scholarship. G. S. S. acknowledges the DALAC for the financial support and NSERC Discovery Grant. Z. W. acknowledges the National Key Research and Development Program of China (2019YFB2203400) and the "111 Project" (B20030).

Conflict of Interest

The authors declare no conflict of interest.

Keywords

core-shell, H_2 generation, heavy-metal-free, LSC, quantum dots, solar cells

[1] J. Tsao, N. Lewis, G. Crabtree, *US Department of Energy* **2006**, *13*, 1.
[2] S. Hadke, M. Huang, C. Chen, Y. F. Tay, S. Chen, J. Tang, L. Wong, *Chem. Rev.* **2022**, *122*, 10170.
[3] F. P. García de Arquer, D. V. Talapin, V. I. Klimov, Y. Arakawa, M. Bayer, E. H. Sargent, *Science* **2021**, *373*, eaaz8541.
[4] G. H. Carey, A. L. Abdelhady, Z. Ning, S. M. Thon, O. M. Bakr, E. H. Sargent, *Chem. Rev.* **2015**, *115*, 12732.
[5] a) Y. Yan, R. W. Crisp, J. Gu, B. D. Chernomordik, G. F. Pach, A. R. Marshall, J. A. Turner, M. C. Beard, *Nat. Energy* **2017**, *2*, 17052; b) M. C. Beard, J. M. Luther, O. E. Semonin, A. J. Nozik, *Acc. Chem. Res.* **2013**, *46*, 1252.
[6] W. A. Tisdale, K. J. Williams, B. A. Timp, D. J. Norris, E. S. Aydil, X. Y. Zhu, *Science* **2010**, *328*, 1543.
[7] O. E. Semonin, J. M. Luther, S. Choi, H.-Y. Chen, J. Gao, A. J. Nozik, M. C. Beard, *Science* **2011**, *334*, 1530.
[8] a) Y. Zhang, G. Wu, F. Liu, C. Ding, Z. Zou, Q. Shen, *Chem. Soc. Rev.* **2020**, *49*, 49; b) G. S. Selopal, H. Zhao, Z. M. Wang, F. Rosei, *Adv. Funct. Mater.* **2020**, *30*, 1908762.
[9] L. Jin, H. Zhao, Z. M. Wang, F. Rosei, *Adv. Energy Mater.* **2021**, *11*, 2003233.
[10] Y. Zhou, H. Zhao, D. Ma, F. Rosei, *Chem. Soc. Rev.* **2018**, *47*, 5866.
[11] P. Kalisman, Y. Nakibli, L. Amirav, *Nano Lett.* **2016**, *16*, 1776.
[12] H. Aqoma, S.-H. Lee, I. F. Imran, J.-H. Hwang, S.-H. Lee, S.-Y. Jang, *Nat. Energy* **2024**, *9*, 324.
[13] I. Coropceanu, M. G. Bawendi, *Nano Lett.* **2014**, *14*, 4097.
[14] H. Li, K. Wu, J. Lim, H.-J. Song, V. I. Klimov, *Nat. Energy* **2016**, *1*, 16157.
[15] Y. Zhou, D. Benetti, Z. Fan, H. Zhao, D. Ma, A. O. Govorov, A. Vomiero, F. Rosei, *Adv. Energy Mater.* **2016**, *6*, 1501913.
[16] H. Ali, E. Khan, I. Ilahi, *J. Chem.* **2019**, *2019*, 6730305.
[17] a) M. Vasilopoulou, H. P. Kim, B. S. Kim, M. Papadakis, A. E. X. Gavim, A. G. Macedo, W. J. da Silva, F. K. Schneider, M. A. M. Teridi, A. G. Coutsolelos, A. R. B. M. Yusoff, *Nat. Photonics* **2020**, *14*, 50; b) Y.-H. Won, O. Cho, T. Kim, D.-Y. Chung, T. Kim, H. Chung, H. Jang, J. Lee, D. Kim, E. Jang, *Nature* **2019**, *575*, 634; c) F. Meinardi, H. McDaniel, F. Carulli, A. Colombo, K. A. Velizhanin, N. S. Makarov, R. Simonutti, V. I. Klimov, S. Brovelli, *Nat. Nanotechnol.* **2015**, *10*, 878; d) T. Kim, K.-H. Kim, S. Kim, S.-M. Choi, H. Jang, H.-K. Seo, H. Lee, D.-Y. Chung, E. Jang, *Nature* **2020**, *586*, 385; e) K. E. Knowles, K. H. Hartstein, T. B. Kilburn, A. Marchioro, H. D. Nelson, P. J. Whitham, D. R. Gamelin, *Chem. Rev.* **2016**, *116*, 10820.
[18] a) A. Brodu, M. D. Tessier, D. Canneson, D. Dupont, M. V. Ballottin, P. C. M. Christianen, C. de Mello Donega, Z. Hens, D. R. Yakovlev, M. Bayer, D. Vanmaekelbergh, L. Biadala, *ACS Nano* **2019**, *13*, 10201; b) K. E. Hughes, J. L. Stein, M. R. Friedfeld, B. M. Cossairt, D. R. Gamelin, *ACS Nano* **2019**, *13*, 14198.
[19] A. F. Richter, M. Binder, B. J. Bohn, N. Grumbach, S. Neyshtadt, A. S. Urban, J. Feldmann, *ACS Nano* **2019**, *13*, 14408.
[20] W. van der Stam, M. de Graaf, S. Gudjonsdottir, J. J. Geuchies, J. J. Dijkema, N. Kirkwood, W. H. Evers, A. Longo, A. J. Houtepen, *ACS Nano* **2018**, *12*, 11244.
[21] a) E. M. Janke, N. E. Williams, C. She, D. Zherebetskyy, M. H. Hudson, L. Wang, D. J. Gosztola, R. D. Schaller, B. Lee, C. Sun, G. S. Engel, D. V. Talapin, *J. Am. Chem. Soc.* **2018**, *140*, 15791; b) V.

Pinchetti, M. Lorenzon, H. McDaniel, R. Lorenzi, F. Meinardi, V. I. Klimov, S. Brovelli, *Nano Lett.* **2017**, *17*, 4508.
[22] K. E. Hughes, S. R. Ostheller, H. D. Nelson, D. R. Gamelin, *Nano Lett.* **2019**, *19*, 1318.
[23] F. Li, M. Zhang, D. Benetti, L. Shi, L. V. Besteiro, H. Zhang, J. Liu, G. Selopal, S. Sun, Z. Wang, Q. Wei, F. Rosei, *Appl. Catal., B* **2021**, *280*, 119402.
[24] M. Jalalah, M. S. Al-Assiri, J. G. Park, *Adv. Energy Mater.* **2018**, *8*, 1703418.
[25] a) J. Du, R. Singh, I. Fedin, A. S. Fuhr, V. I. Klimov, *Nat. Energy* **2020**, *5*, 409; b) S. Yu, X.-B. Fan, X. Wang, J. Li, Q. Zhang, A. Xia, S. Wei, L.-Z. Wu, Y. Zhou, G. R. Patzke, *Nat. Commun.* **2018**, *9*, 4009.
[26] a) S. Jain, S. Bharti, G. K. Bhullar, S. K. Tripathi, *J. Lumin.* **2020**, *219*, 116912; b) Y. You, X. Tong, W. Wang, J. Sun, P. Yu, H. Ji, X. Niu, Z. M. Wang, *Adv. Sci.* **2019**, *6*, 1801967; c) Z. Li, A. I. Channa, Z. M. Wang, X. Tong, *Small* **2023**, *19*, 2305146.
[27] a) J. M. Pietryga, Y.-S. Park, J. Lim, A. F. Fidler, W. K. Bae, S. Brovelli, V. I. Klimov, *Chem. Rev.* **2016**, *116*, 10513; b) J. Y. Kim, O. Voznyy, D. Zhitomirsky, E. H. Sargent, *Adv. Mater.* **2013**, *25*, 4986; c) H. Lu, Z. Huang, M. S. Martinez, J. C. Johnson, J. M. Luther, M. C. Beard, *Energy Environ. Sci.* **2020**, *13*, 1347; d) C. R. Kagan, E. Lifshitz, E. H. Sargent, D. V. Talapin, *Science* **2016**, *353*, aac5523.
[28] a) H. Zhao, F. Rosei, *Chem* **2017**, *3*, 229; b) E. H. Sargent, *Nat. Photonics* **2012**, *6*, 133; c) Y. Yu, T. Ma, H. Huang, *Adv. Funct. Mater.* **2023**, *33*, 2213770.
[29] A. Tubtimtae, K.-L. Wu, H.-Y. Tung, M.-W. Lee, G. J. Wang, *Electrochem. Commun.* **2010**, *12*, 1158.
[30] A. Tubtimtae, M.-W. Lee, G.-J. Wang, *J. Power Sources* **2011**, *196*, 6603.
[31] J.-Y. Jung, K. Zhou, J. H. Bang, J.-H. Lee, *J. Phys. Chem. C* **2012**, *116*, 12409.
[32] B. Chon, S. Choi, Y. Seo, H. S. Lee, C. H. Kim, H.-J. Son, S. O. Kang, *ACS Sustainable Chem. Eng.* **2022**, *10*, 6033.
[33] F. S. Mirahmadi, M. Marandi, M. Karimipour, M. Molaei, *Sol. Energy* **2020**, *202*, 155.
[34] H. Zhao, X. Li, M. Cai, C. Liu, Y. You, R. Wang, A. I. Channa, F. Lin, D. Huo, G. Xu, X. Tong, Z. M. Wang, *Adv. Energy Mater.* **2021**, *11*, 2101230.
[35] S. Sadeghi, H. Bahmani Jalali, R. Melikov, B. Ganesh Kumar, M. Mohammadi Aria, C. W. Ow-Yang, S. Nizamoglu, *ACS Appl. Mater. Interfaces* **2018**, *10*, 12975.
[36] S. Ren, M. Wang, X. Wang, G. Han, Y. Zhang, H. Zhao, A. Vomiero, *Nanoscale* **2021**, *13*, 3519.
[37] H. Zhao, W. Wang, X. Li, P. Li, M. Cai, Y. You, R. Wang, A. I. Channa, X. Tong, Z. M. Wang, *Adv. Energy Sustainability Res.* **2023**, *4*, 2200142.
[38] M. Cai, X. Tong, H. Zhao, P. Liao, L. Pan, G. Li, Z. M. Wang, *Appl. Catal., B* **2024**, *343*, 123572.
[39] M. G. Panthani, V. Akhavan, B. Goodfellow, J. P. Schmidtke, L. Dunn, A. Dodabalapur, P. F. Barbara, B. A. Korgel, *J. Am. Chem. Soc.* **2008**, *130*, 16770.
[40] L. Shi, X. Ren, Z. Zhang, Q. Wang, Y. Li, J. Ye, *J. Catal.* **2021**, *401*, 271.
[41] a) C. Kim, I. Kozakci, J. Kim, S. Y. Lee, J.-Y. Lee, *Adv. Energy Mater.* **2022**, *12*, 2200262; b) Y. Wang, L. Peng, Z. Wang, G. Konstantatos, *Adv. Energy Mater.* **2022**, *12*, 2200700; c) D. Kim, G. Cho, Y. H. Kim, J. H. Kwon, Y. Oh, M. Yang, S. Jee, I. S. Lee, M.-J. Si, Y. Jung, H. Y. Yang, Y. Ahn, B.-K. Kim, C. Kim, H. S. Kim, S.-W. Baek, *Adv. Energy Mater.* **2024**, *14*, 2302579; d) Y. Wang, S. R. Kavanagh, I. Burgués-Ceballos, A. Walsh, D. O. Scanlon, G. Konstantatos, *Nat. Photonics* **2022**, *16*, 235; e) M. Bernechea, N. Cates, G. Xercavins, D. So, A. Stavrinadis, G. Konstantatos, *Nat. Photonics* **2016**, *10*, 521.
[42] M. R. Bergren, N. S. Makarov, K. Ramasamy, A. Jackson, R. Guglielmetti, H. McDaniel, *ACS Energy Lett.* **2018**, *3*, 520.
[43] B. Bhattacharyya, A. K. Simlandy, A. Chakraborty, G. P. Rajasekar, N. B. Aetukuri, S. Mukherjee, A. Pandey, *ACS Energy Lett.* **2018**, *3*, 1508.
[44] S. M. Kobosko, D. H. Jara, P. V. Kamat, *ACS Appl. Mater. Interfaces* **2017**, *9*, 33379.
[45] M. A. Abate, J.-Y. Chang, *Sol. Energy Mater. Sol. Cells* **2018**, *182*, 37.
[46] Z. Long, X. Tong, R. Wang, A. I. Channa, X. Li, Y. You, L. Xia, M. Cai, H. Zhao, Z. M. Wang, *ChemSusChem* **2022**, *15*, 202200346.
[47] W. Li, Z. Pan, X. Zhong, *J. Mater. Chem. A* **2015**, *3*, 1649.
[48] X. Tong, X. T. Kong, Y. Zhou, F. Navarro-Pardo, G. S. Selopal, S. Sun, A. O. Govorov, H. Zhao, Z. M. Wang, F. Rosei, *Adv. Energy Mater.* **2018**, *8*, 1701432.
[49] L. Jin, J. Liu, X. Liu, D. Benetti, G. S. Selopal, X. Tong, E. Hamzehpoor, F. Li, D. F. Perepichka, Z. M. Wang, F. Rosei, *Small Methods* **2023**, *8*, 2300133.
[50] a) J. Du, Z. Du, J.-S. Hu, Z. Pan, Q. Shen, J. Sun, D. Long, H. Dong, L. Sun, X. Zhong, L.-J. Wan, *J. Am. Chem. Soc.* **2016**, *138*, 4201; b) W. Wang, W. Feng, J. Du, W. Xue, L. Zhang, L. Zhao, Y. Li, X. Zhong, *Adv. Mater.* **2018**, *30*, 1705746.
[51] Z. Pan, L. Yue, H. Rao, J. Zhang, X. Zhong, Z. Zhu, A. K. Y. Jen, *Adv. Mater.* **2019**, *31*, 1903696.
[52] Y.-J. Yuan, D.-Q. Chen, M. Xiong, J.-S. Zhong, Z.-Y. Wan, Y. Zhou, S. Liu, Z.-T. Yu, L.-X. Yang, Z.-G. Zou, *Appl. Catal., B* **2017**, *204*, 58.
[53] X. Tong, Y. Zhou, L. Jin, K. Basu, R. Adhikari, G. S. Selopal, X. Tong, H. Zhao, S. Sun, A. Vomiero, Z. M. Wang, F. Rosei, *Nano Energy* **2017**, *31*, 441.
[54] C. Steinhagen, M. G. Panthani, V. Akhavan, B. Goodfellow, B. Koo, B. A. Korgel, *J. Am. Chem. Soc.* **2009**, *131*, 12554.
[55] Y. You, X. Tong, A. I. Channa, H. Zhi, M. Cai, H. Zhao, L. Xia, G. Liu, H. Zhao, Z. Wang, *Chem. Eng. J.* **2023**, *452*, 139490.
[56] H. Zhi, X. Tong, Y. You, A. I. Channa, X. Li, J. Wu, G. S. Selopal, Z. M. Wang, *Sol. RRL* **2023**, *7*, 2300641.
[57] H. Guo, B. Luo, J. Wang, B. Wang, X. Huang, J. Yang, W. Gong, Y. Zhou, X. Niu, *J. Mater. Chem. A* **2020**, *8*, 24655.
[58] L. Yue, H. Rao, J. Du, Z. Pan, J. Yu, X. Zhong, *RSC Adv.* **2018**, *8*, 3637.
[59] H. Rao, M. Zhou, Z. Pan, X. Zhong, *J. Mater. Chem. A* **2020**, *8*, 10233.
[60] a) H. Song, Y. Lin, Z. Zhang, H. Rao, W. Wang, Y. Fang, Z. Pan, X. Zhong, *J. Am. Chem. Soc.* **2021**, *143*, 4790; b) Z. Zhang, H. Song, W. Wang, H. Rao, Y. Fang, Z. Pan, X. Zhong, *ACS Energy Lett.* **2023**, *8*, 647.
[61] M. Zhu, Y. Li, S. Tian, Y. Xie, X. Zhao, X. Gong, *J. Colloid Interface Sci.* **2019**, *534*, 509.
[62] S. Sadeghi, H. B. Jalali, S. B. Srivastava, R. Melikov, I. Baylam, A. Sennaroglu, S. Nizamoglu, *iScience* **2020**, *23*, 101272.
[63] J. Bang, S. Das, E.-J. Yu, K. Kim, H. Lim, S. Kim, J. W. Hong, *Nano Lett.* **2020**, *20*, 6263.
[64] X. Liu, B. Luo, J. Liu, D. Jing, D. Benetti, F. Rosei, *J. Mater. Chem. A* **2020**, *8*, 1787.
[65] R. Wang, X. Tong, A. I. Channa, Q. Zeng, J. Sun, C. Liu, X. Li, J. Xu, F. Lin, G. S. Selopal, F. Rosei, Y. Zhang, J. Wu, H. Zhao, A. Vomiero, X. Sun, Z. M. Wang, *J. Mater. Chem. A* **2020**, *8*, 10736.
[66] R. Wang, X. Tong, Z. Long, A. I. Channa, H. Zhao, X. Li, M. Cai, Y. You, X. Sun, Z. Wang, *Nano Res.* **2022**, *15*, 7614.
[67] L. Xia, X. Tong, X. Li, A. I. Channa, Y. You, Z. Long, A. Vomiero, Z. M. Wang, *Chem. Eng. J.* **2022**, *442*, 136214.
[68] L. Xia, X. Tong, Y. Yao, Z. Long, M. Cai, L. Jin, A. Vomiero, Z. M. Wang, *Nano Energy* **2024**, *122*, 109302.
[69] R. Rossetti, L. Brus, *J. Phys. Chem.* **1982**, *86*, 4470.
[70] A. P. Alivisatos, *Science* **1996**, *271*, 933.
[71] V. I. Klimov, D. W. McBranch, *Phys. Rev. Lett.* **1998**, *80*, 4028.
[72] L. Jin, G. Sirigu, X. Tong, A. Camellini, A. Parisini, G. Nicotra, C. Spinella, H. Zhao, S. Sun, V. Morandi, M. Zavelani-Rossi, F. Rosei, A. Vomiero, *Nano Energy* **2016**, *30*, 531.
[73] R. E. Bailey, S. Nie, *J. Am. Chem. Soc.* **2003**, *125*, 7100.

[74] R. Marin, D. Jaque, *Chem. Rev.* **2021**, *121*, 1425.
[75] L. Jin, E. Hamzehpoor, G. S. Selopal, J. Liu, P. Kumar, D. Benetti, X. Tong, D. F. Perepichka, Z. M. Wang, F. Rosei, *Small Methods* **2024**, *44*, 2301695.
[76] N. Pradhan, D. Goorskey, J. Thessing, X. Peng, *J. Am. Chem. Soc.* **2005**, *127*, 17586.
[77] S. C. Erwin, L. Zu, M. I. Haftel, A. L. Efros, T. A. Kennedy, D. J. Norris, *Nature* **2005**, *436*, 91.
[78] N. Pradhan, X. Peng, *J. Am. Chem. Soc.* **2007**, *129*, 3339.
[79] D. J. Norris, N. Yao, F. T. Charnock, T. A. Kennedy, *Nano Lett.* **2001**, *1*, 3.
[80] a) B. B. Srivastava, S. Jana, N. Pradhan, *J. Am. Chem. Soc.* **2011**, *133*, 1007; b) R. Xie, X. Peng, *J. Am. Chem. Soc.* **2009**, *131*, 10645.
[81] H. D. Nelson, S. O. M. Hinterding, R. Fainblat, S. E. Creutz, X. Li, D. R. Gamelin, *J. Am. Chem. Soc.* **2017**, *139*, 6411.
[82] N. S. Norberg, G. L. Parks, G. M. Salley, D. R. Gamelin, *J. Am. Chem. Soc.* **2006**, *128*, 13195.
[83] W. Yang, W. Guo, X. Gong, B. Zhang, S. Wang, N. Chen, W. Yang, Y. Tu, X. Fang, J. Chang, *ACS Appl. Mater. Interfaces* **2015**, *7*, 18759.
[84] O. E. Raola, G. F. Strouse, *Nano Lett.* **2002**, *2*, 1443.
[85] C. S. Erickson, L. R. Bradshaw, S. McDowall, J. D. Gilbertson, D. R. Gamelin, D. L. Patrick, *ACS Nano* **2014**, *8*, 3461.
[86] G. Manna, S. Jana, R. Bose, N. Pradhan, *J. Phys. Chem. Lett.* **2012**, *3*, 2528.
[87] T. A. Kennedy, E. R. Glaser, P. B. Klein, R. N. Bhargava, *Phys. Rev. B* **1995**, *52*, 14356.
[88] X. Yuan, R. Ma, W. Zhang, J. Hua, X. Meng, X. Zhong, J. Zhang, J. Zhao, H. Li, *ACS Appl. Mater. Interfaces* **2015**, *7*, 8659.
[89] a) V. Srivastava, V. Kamysbayev, L. Hong, E. Dunietz, R. F. Klie, D. V. Talapin, *J. Am. Chem. Soc.* **2018**, *140*, 12144; b) Q. A. Akkerman, A. Genovese, C. George, M. Prato, I. Moreels, A. Casu, S. Marras, A. Curcio, A. Scarpellini, T. Pellegrino, L. Manna, V. Lesnyak, *ACS Nano* **2015**, *9*, 521; c) H. Song, Y. Lin, M. Zhou, H. Rao, Z. Pan, X. Zhong, *Angew. Chem., Int. Ed.* **2021**, *60*, 6137.
[90] S.-W. Kim, J. P. Zimmer, S. Ohnishi, J. B. Tracy, J. V. Frangioni, M. G. Bawendi, *J. Am. Chem. Soc.* **2005**, *127*, 10526.
[91] K.-H. Kim, J.-H. Jo, D.-Y. Jo, C.-Y. Han, S.-Y. Yoon, Y. Kim, Y.-H. Kim, Y. H. Ko, S. W. Kim, C. Lee, H. Yang, *Chem. Mater.* **2020**, *32*, 3537.
[92] a) F. Pietra, L. De Trizio, A. W. Hoekstra, N. Renaud, M. Prato, F. C. Grozema, P. J. Baesjou, R. Koole, L. Manna, A. J. Houtepen, *ACS Nano* **2016**, *10*, 4754; b) J. P. Park, J.-J. Lee, S.-W. Kim, *J. Am. Chem. Soc.* **2016**, *138*, 16568; c) M. Rafipoor, D. Dupont, H. Tornatzky, M. D. Tessier, J. Maultzsch, Z. Hens, H. Lange, *Chem. Mater.* **2018**, *30*, 4393.
[93] J. Lim, W. K. Bae, D. Lee, M. K. Nam, J. Jung, C. Lee, K. Char, S. Lee, *Chem. Mater.* **2011**, *23*, 4459.
[94] O. Yarema, M. Yarema, V. Wood, *Chem. Mater.* **2018**, *30*, 1446.
[95] W. Chen, J. Li, P. Liu, H. Liu, J. Xia, S. Li, D. Wang, D. Wu, W. Lu, X. W. Sun, K. Wang, *Sol. RRL* **2017**, *1*, 1700041.
[96] J. Zhang, R. Xie, W. Yang, *Chem. Mater.* **2011**, *23*, 3357.
[97] P. M. Allen, M. G. Bawendi, *J. Am. Chem. Soc.* **2008**, *130*, 9240.
[98] J. F. L. Lox, Z. Dang, V. M. Dzhagan, D. Spittel, B. Martín-García, I. Moreels, D. R. T. Zahn, V. Lesnyak, *Chem. Mater.* **2018**, *30*, 2607.
[99] L. Wang, Z. Chen, G. Liang, Y. Li, R. Lai, T. Ding, K. Wu, *Nat. Commun.* **2019**, *10*, 4532.
[100] A. Aboulaich, L. Balan, J. Ghanbaja, G. Medjahdi, C. Merlin, R. Schneider, *Chem. Mater.* **2011**, *23*, 3706.
[101] S.-Y. Yoon, J.-H. Kim, E.-P. Jang, S.-H. Lee, D.-Y. Jo, Y. Kim, Y. R. Do, H. Yang, *Chem. Mater.* **2019**, *31*, 2627.
[102] H. Zhu, N. Song, T. Lian, *J. Am. Chem. Soc.* **2010**, *132*, 15038.
[103] H. Zhao, Z. Fan, H. Liang, G. S. Selopal, B. A. Gonfa, L. Jin, A. Soudi, D. Cui, F. Enrichi, M. M. Natile, I. Concina, D. Ma, A. O. Govorov, F. Rosei, A. Vomiero, *Nanoscale* **2014**, *6*, 7004.
[104] L. P. Balet, S. A. Ivanov, A. Piryatinski, M. Achermann, V. I. Klimov, *Nano Lett.* **2004**, *4*, 1485.
[105] L. A. Swafford, L. A. Weigand, M. J. Bowers, J. R. McBride, J. L. Rapaport, T. L. Watt, S. K. Dixit, L. C. Feldman, S. J. Rosenthal, *J. Am. Chem. Soc.* **2006**, *128*, 12299.
[106] a) S. Kim, B. Fisher, H.-J. Eisler, M. Bawendi, *J. Am. Chem. Soc.* **2003**, *125*, 11466; b) S. A. Ivanov, A. Piryatinski, J. Nanda, S. Tretiak, K. R. Zavadil, W. O. Wallace, D. Werder, V. I. Klimov, *J. Am. Chem. Soc.* **2007**, *129*, 11708.
[107] F. Meinardi, A. Colombo, K. A. Velizhanin, R. Simonutti, M. Lorenzon, L. Beverina, R. Viswanatha, V. I. Klimov, S. Brovelli, *Nat. Photonics* **2014**, *8*, 392.
[108] H. Zhu, N. Song, H. Lv, C. L. Hill, T. Lian, *J. Am. Chem. Soc.* **2012**, *134*, 11701.
[109] a) Y. Chen, J. Vela, H. Htoon, J. L. Casson, D. J. Werder, D. A. Bussian, V. I. Klimov, J. A. Hollingsworth, *J. Am. Chem. Soc.* **2008**, *130*, 5026; b) Y. Ghosh, B. D. Mangum, J. L. Casson, D. J. Williams, H. Htoon, J. A. Hollingsworth, *J. Am. Chem. Soc.* **2012**, *134*, 9634; c) J. J. Li, Y. A. Wang, W. Guo, J. C. Keay, T. D. Mishima, M. B. Johnson, X. Peng, *J. Am. Chem. Soc.* **2003**, *125*, 12567.
[110] J. M. Pietryga, D. J. Werder, D. J. Williams, J. L. Casson, R. D. Schaller, V. I. Klimov, J. A. Hollingsworth, *J. Am. Chem. Soc.* **2008**, *130*, 4879.
[111] a) L. Jin, B. AlOtaibi, D. Benetti, S. Li, H. Zhao, Z. Mi, A. Vomiero, F. Rosei, *Adv. Sci.* **2016**, *3*, 1500345; b) R. Adhikari, L. Jin, F. Navarro-Pardo, D. Benetti, B. AlOtaibi, S. Vanka, H. Zhao, Z. Mi, A. Vomiero, F. Rosei, *Nano Energy* **2016**, *27*, 265.
[112] L. Liu, H. Li, Z. Liu, Y.-H. Xie, *J. Colloid Interface Sci.* **2019**, *546*, 276.
[113] P. Reiss, M. Protiere, L. Li, *Small* **2009**, *5*, 154.
[114] M. D. Tessier, E. A. Baquero, D. Dupont, V. Grigel, E. Bladt, S. Bals, Y. Coppel, Z. Hens, C. Nayral, F. Delpech, *Chem. Mater.* **2018**, *30*, 6877.
[115] a) Y. Li, X. Hou, X. Dai, Z. Yao, L. Lv, Y. Jin, X. Peng, *J. Am. Chem. Soc.* **2019**, *141*, 6448; b) F. Cao, S. Wang, F. Wang, Q. Wu, D. Zhao, X. Yang, *Chem. Mater.* **2018**, *30*, 8002.
[116] S.-H. Wei, A. Zunger, *Appl. Phys. Lett.* **1998**, *72*, 2011.
[117] B. Ji, Y. E. Panfil, N. Waiskopf, S. Remennik, I. Popov, U. Banin, *Nat. Commun.* **2019**, *10*, 1.
[118] D. Hahm, J. H. Chang, B. G. Jeong, P. Park, J. Kim, S. Lee, J. Choi, W. D. Kim, S. Rhee, J. Lim, D. C. Lee, C. Lee, K. Char, W. K. Bae, *Chem. Mater.* **2019**, *31*, 3476.
[119] L. K. Sagar, G. Bappi, A. Johnston, B. Chen, P. Todorovic´, L. Levina, M. I. Saidaminov, F. P. García de Arquer, S. Hoogland, E. H. Sargent, *Chem. Mater.* **2020**, *32*, 2919.
[120] S.-H. Lee, C.-Y. Han, S.-W. Song, D.-Y. Jo, J.-H. Jo, S.-Y. Yoon, H.-M. Kim, S. Hong, J. Y. Hwang, H. Yang, *Chem. Mater.* **2020**, *32*, 5768.
[121] a) C. Burda, X. Chen, R. Narayanan, M. A. El-Sayed, *Chem. Rev.* **2005**, *105*, 1025; b) J. Park, Y. H. Won, Y. Han, H. M. Kim, E. Jang, D. Kim, *Small* **2022**, *18*, 2105492.
[122] a) H. Zang, H. Li, N. S. Makarov, K. A. Velizhanin, K. Wu, Y.-S. Park, V. I. Klimov, *Nano Lett.* **2017**, *17*, 1787; b) E. Cassette, B. Mahler, J.-M. Guigner, G. Patriarche, B. Dubertret, T. Pons, *ACS Nano* **2012**, *6*, 6741.
[123] B. Mahler, N. Lequeux, B. Dubertret, *J. Am. Chem. Soc.* **2010**, *132*, 953.
[124] M.-A. Langevin, A. M. Ritcey, C. N. Allen, *ACS Nano* **2014**, *8*, 3476.
[125] M. D. Tessier, D. Dupont, K. De Nolf, J. De Roo, Z. Hens, *Chem. Mater.* **2015**, *27*, 4893.
[126] H. McDaniel, A. Y. Koposov, S. Draguta, N. S. Makarov, J. M. Pietryga, V. I. Klimov, *J. Phys. Chem. C* **2014**, *118*, 16987.
[127] G. S. Selopal, H. Zhao, X. Tong, D. Benetti, F. Navarro-Pardo, Y. Zhou, D. Barba, F. Vidal, Z. M. Wang, F. Rosei, *Adv. Funct. Mater.* **2017**, *27*, 1701468.

[128] X. Tong, X. T. Kong, C. Wang, Y. Zhou, F. Navarro-Pardo, D. Barba, D. Ma, S. Sun, A. O. Govorov, H. Zhao, Z. M. Wang, F. Rosei, *Adv. Sci.* **2018**, *5*, 1800656.
[129] K. R. Reid, J. R. McBride, N. J. Freymeyer, L. B. Thal, S. J. Rosenthal, *Nano Lett.* **2018**, *18*, 709.
[130] C. E. Rowland, W. Liu, D. C. Hannah, M. K. Y. Chan, D. V. Talapin, R. D. Schaller, *ACS Nano* **2014**, *8*, 977.
[131] P. Liu, Y. Lou, S. Ding, W. Zhang, Z. Wu, H. Yang, B. Xu, K. Wang, X. W. Sun, *Adv. Funct. Mater.* **2021**, *31*, 2008453.
[132] J. van Embden, P. Mulvaney, *Langmuir* **2005**, *21*, 10226.
[133] J. Huang, M. V. Kovalenko, D. V. Talapin, *J. Am. Chem. Soc.* **2010**, *132*, 15866.
[134] A. Heuer-Jungemann, N. Feliu, I. Bakaimi, M. Hamaly, A. Alkilany, I. Chakraborty, A. Masood, M. F. Casula, A. Kostopoulou, E. Oh, K. Susumu, M. H. Stewart, I. L. Medintz, E. Stratakis, W. J. Parak, A. G. Kanaras, *Chem. Rev.* **2019**, *119*, 4819.
[135] K. Kim, D. Yoo, H. Choi, S. Tamang, J.-H. Ko, S. Kim, Y.-H. Kim, S. Jeong, *Angew. Chem., Int. Ed.* **2016**, *55*, 3714.
[136] L. Qu, X. Peng, *J. Am. Chem. Soc.* **2002**, *124*, 2049.
[137] J. Jasieniak, M. Califano, S. E. Watkins, *ACS Nano* **2011**, *5*, 5888.
[138] P. R. Brown, D. Kim, R. R. Lunt, N. Zhao, M. G. Bawendi, J. C. Grossman, V. Bulovic, *ACS Nano* **2014**, *8*, 5863.
[139] D. M. Kroupa, M. Vörös, N. P. Brawand, B. W. McNichols, E. M. Miller, J. Gu, A. J. Nozik, A. Sellinger, G. Galli, M. C. Beard, *Nat. Commun.* **2017**, *8*, 15257.
[140] H. Zhang, W. Fang, W. Wang, N. Qian, X. Ji, *ACS Appl. Mater. Interfaces* **2019**, *11*, 6927.
[141] M. V. Kovalenko, M. Scheele, D. V. Talapin, *Science* **2009**, *324*, 1417.
[142] G. Konstantatos, I. Howard, A. Fischer, S. Hoogland, J. Clifford, E. Klem, L. Levina, E. H. Sargent, *Nature* **2006**, *442*, 180.
[143] a) M. J. Greaney, E. Couderc, J. Zhao, B. A. Nail, M. Mecklenburg, W. Thornbury, F. E. Osterloh, S. E. Bradforth, R. L. Brutchey, *Chem. Mater.* **2015**, *27*, 744; b) J. Tang, K. W. Kemp, S. Hoogland, K. S. Jeong, H. Liu, L. Levina, M. Furukawa, X. Wang, R. Debnath, D. Cha, K. Chou, A. Fischer, A. Amassian, J. B. Asbury, E. H. Sargent, *Nat. Mater.* **2011**, *10*, 765.
[144] S. Lian, D. J. Weinberg, R. D. Harris, M. S. Kodaimati, E. A. Weiss, *ACS Nano* **2016**, *10*, 6372.
[145] M. Califano, *J. Phys. Chem. Lett.* **2020**, *11*, 280.
[146] a) J. Owen, L. Brus, *J. Am. Chem. Soc.* **2017**, *139*, 10939; b) P. Reiss, M. Carriere, C. Lincheneau, L. Vaure, S. Tamang, *Chem. Rev.* **2016**, *116*, 10731.
[147] S. Hinds, S. Myrskog, L. Levina, G. Koleilat, J. Yang, S. O. Kelley, E. H. Sargent, *J. Am. Chem. Soc.* **2007**, *129*, 7218.
[148] a) X. Wang, M. T. Swihart, *Chem. Mater.* **2015**, *27*, 1786; b) L. Li, M. Protière, P. Reiss, *Chem. Mater.* **2008**, *20*, 2621.
[149] J. van Embden, A. S. R. Chesman, J. J. Jasieniak, *Chem. Mater.* **2015**, *27*, 2246.
[150] H. Nishimura, Y. Lin, M. Hizume, T. Taniguchi, N. Shigekawa, T. Takagi, S. Sobue, S. Kawai, E. Okuno, D. Kim, *Chem. Lett.* **2019**, *48*, 1081.
[151] C. Xia, J. D. Meeldijk, H. C. Gerritsen, C. de Mello Donega, *Chem. Mater.* **2017**, *29*, 4940.
[152] W. Van Der Stam, A. C. Berends, F. T. Rabouw, T. Willhammar, X. Ke, J. D. Meeldijk, S. Bals, C. de Mello Donega, *Chem. Mater.* **2015**, *27*, 621.
[153] L. Li, P. Reiss, *J. Am. Chem. Soc.* **2008**, *130*, 11588.
[154] J. Ning, S. V. Kershaw, A. L. Rogach, *J. Am. Chem. Soc.* **2019**, *141*, 20516.
[155] V. Grigel, D. Dupont, K. De Nolf, Z. Hens, M. D. Tessier, *J. Am. Chem. Soc.* **2016**, *138*, 13485.
[156] X. Peng, J. Wickham, A. P. Alivisatos, *J. Am. Chem. Soc.* **1998**, *120*, 5343.
[157] A. C. Berends, W. Van Der Stam, J. P. Hofmann, E. Bladt, J. D. Meeldijk, S. Bals, C. de Mello Donega, *Chem. Mater.* **2018**, *30*, 2400.
[158] S. Kim, T. Kim, M. Kang, S. K. Kwak, T. W. Yoo, L. S. Park, I. Yang, S. Hwang, J. E. Lee, S. K. Kim, S.-W. Kim, *J. Am. Chem. Soc.* **2012**, *134*, 3804.
[159] F. Pietra, N. Kirkwood, L. De Trizio, A. W. Hoekstra, L. Kleibergen, N. Renaud, R. Koole, P. Baesjou, L. Manna, A. J. Houtepen, *Chem. Mater.* **2017**, *29*, 5192.
[160] J. Ning, Y. Xiong, F. Huang, Z. Duan, S. V. Kershaw, A. L. Rogach, *Chem. Mater.* **2020**, *32*, 7842.
[161] W. Han, L. Yi, N. Zhao, A. Tang, M. Gao, Z. Tang, *J. Am. Chem. Soc.* **2008**, *130*, 13152.
[162] J. Ning, Z. Duan, S. V. Kershaw, A. L. Rogach, *ACS Nano* **2020**, *14*, 11799.
[163] P. K. Jain, L. Amirav, S. Aloni, A. P. Alivisatos, *J. Am. Chem. Soc.* **2010**, *132*, 9997.
[164] K. Miszta, D. Dorfs, A. Genovese, M. R. Kim, L. Manna, *ACS Nano* **2011**, *5*, 7176.
[165] H. Li, R. Brescia, R. Krahne, G. Bertoni, M. J. P. Alcocer, C. D'Andrea, F. Scotognella, F. Tassone, M. Zanella, M. De Giorgi, L. Manna, *ACS Nano* **2012**, *6*, 1637.
[166] A. M. O. I. Zaban, O. I. Mićić, B. A. Gregg, A. J. Nozik, *Langmuir* **1998**, *14*, 3153.
[167] *Best Research-Cell Efficiency Chart*, https://www.nrel.gov/pv/cell-efficiency.html (accessed: June 2024).
[168] S.-W. Baek, S. Jun, B. Kim, A. H. Proppe, O. Ouellette, O. Voznyy, C. Kim, J. Kim, G. Walters, J. H. Song, S. Jeong, H. R. Byun, M. S. Jeong, S. Hoogland, F. P. García de Arquer, O. S. Kelley, J.-Y. Lee, E. H. Sargent, *Nat. Energy* **2019**, *4*, 969.
[169] G. Shi, A. Kaewprajak, X. Ling, A. Hayakawa, S. Zhou, B. Song, Y. Kang, T. Hayashi, M. E. Altun, M. Nakaya, Z. Liu, H. Wang, T. Sagawa, W. Ma, *ACS Energy Lett.* **2019**, *4*, 960.
[170] Z. Pan, H. Rao, I. Mora-Seró, J. Bisquert, X. Zhong, *Chem. Soc. Rev.* **2018**, *47*, 7659.
[171] K. Zhao, Z. Pan, X. Zhong, *J. Phys. Chem. Lett.* **2016**, *7*, 406.
[172] I. Mora-Sero, S. Giménez, F. Fabregat-Santiago, R. Gómez, Q. Shen, T. Toyoda, J. Bisquert, *Acc. Chem. Res.* **2009**, *42*, 1848.
[173] a) K.-T. Kuo, D.-M. Liu, S.-Y. Chen, C.-C. Lin, *J. Mater. Chem.* **2009**, *19*, 6780; b) Z. Pan, I. N. Mora-Seró, Q. Shen, H. Zhang, Y. Li, K. Zhao, J. Wang, X. Zhong, J. Bisquert, *J. Am. Chem. Soc.* **2014**, *136*, 9203; c) W. Zhu, Y.-Y. Hu, W. Wang, Y. Xie, W. Xue, F. He, Y. Li, *ACS Appl. Energy Mater.* **2021**, *4*, 5767.
[174] V. Chakrapani, D. Baker, P. V. Kamat, *J. Am. Chem. Soc.* **2011**, *133*, 9607.
[175] A. Raevskaya, O. Rosovik, A. Kozytskiy, O. Stroyuk, V. Dzhagan, D. R. T. Zahn, *RSC Adv.* **2016**, *6*, 100145.
[176] L. Mehdaoui, R. Miloua, M. Khadraoui, M. O. Bensaid, D. Abdelkader, F. Chiker, A. Bouzidi, *Phys. B* **2019**, *564*, 114.
[177] W. Wang, L. Zhao, Y. Wang, W. Xue, F. He, Y. Xie, Y. Li, *J. Am. Chem. Soc.* **2019**, *141*, 4300.
[178] S. M. Kobosko, P. V. Kamat, *J. Phys. Chem. C* **2018**, *122*, 14336.
[179] G. Halder, A. Ghosh, S. Parvin, S. Bhattacharyya, *Chem. Mater.* **2019**, *31*, 161.
[180] Y. W. Han, S. J. Jeon, J. Y. Choi, J. H. Kim, D. K. Moon, *Sol. RRL* **2018**, *2*, 1800077.
[181] Z. Li, X. Zhang, C. Liu, Z. Zhang, Y. He, J. Li, L. Shen, W. Guo, S. Ruan, *J. Phys. Chem. C* **2015**, *119*, 26747.
[182] R. Peng, T. Yan, J. Chen, S. Yang, Z. Ge, M. Wang, *Adv. Electron. Mater.* **2020**, *6*, 1901245.
[183] a) B. McKenna, R. C. Evans, *Adv. Mater.* **2017**, *29*, 1606491; b) X. Huang, S. Han, W. Huang, X. Liu, *Chem. Soc. Rev.* **2013**, *42*, 173.
[184] M. G. Debije, P. P. C. Verbunt, *Adv. Energy Mater.* **2012**, *2*, 12.
[185] B. G. Jeong, D. Hahm, J. W. Park, J. Y. Kim, H.-E. Song, M. G. Kang, S. Jeong, G. Kang, W. K. Bae, H.-J. Song, *Nano Energy* **2020**, *77*, 105169.

[186] J. H. Kim, D. Hansora, P. Sharma, J.-W. Jang, J. S. Lee, *Chem. Soc. Rev.* **2019**, *48*, 1908.
[187] A. Fujishima, K. Honda, *Nature* **1972**, *238*, 37.
[188] D. K. I. Lee, D. Lee, M. A. Lumley, K.-S. Choi, *Chem. Soc. Rev.* **2019**, *48*, 2126.
[189] X. Tong, A. I. Channa, Y. You, P. Wei, X. Li, F. Lin, J. Wu, A. Vomiero, Z. M. Wang, *Nano Energy* **2020**, *76*, 105062.
[190] M. Sandroni, R. Gueret, K. D. Wegner, P. Reiss, J. Fortage, D. Aldakov, M.-N. Collomb, *Energy Environ. Sci.* **2018**, *11*, 1752.
[191] Z. Han, R. Eisenberg, *Acc. Chem. Res.* **2014**, *47*, 2537.
[192] R. Van de Krol, M. Grätzel, *Photoelectrochemical Hydrogen Production*, Vol. *90*, Springer, New York **2012**.
[193] C. Nie, W. Ni, L. Gong, J. Jiang, J. Wang, M. Wang, *J. Mater. Chem. A* **2019**, *7*, 27432.
[194] M. Cai, X. Li, H. Zhao, C. Liu, Y. You, F. Lin, X. Tong, Z. M. Wang, *ACS Appl. Mater. Interfaces* **2021**, *13*, 50046.
[195] X.-B. Li, C.-H. Tung, L.-Z. Wu, *Nat. Rev. Chem.* **2018**, *2*, 160.
[196] A. J. Bard, M. A. Fox, *Acc. Chem. Res.* **1995**, *28*, 141.
[197] K. Basu, H. Zhang, H. Zhao, S. Bhattacharya, F. Navarro-Pardo, P. K. Datta, L. Jin, S. Sun, F. Vetrone, F. Rosei, *Nanoscale* **2018**, *10*, 15273.
[198] G. Liu, B. Sun, H. Li, Y. Wang, H. Zhao, *J. Mater. Chem. A* **2019**, *7*, 18529.
[199] M. Cai, X. Tong, H. Zhao, X. Li, Y. You, R. Wang, L. Xia, N. Zhou, L. Wang, Z. M. Wang, *Small* **2022**, *18*, 2204495.
[200] J. Huang, B. Xu, L. Tian, P. B. Pati, A. S. Etman, J. Sun, L. Hammarstrom, H. Tian, *Chem. Commun.* **2019**, *55*, 7918.
[201] M. Cai, X. Tong, P. Liao, S. Shen, H. Zhao, X. Li, L. Xia, H. Zhi, N. Zhou, Z. Xue, L. Jin, J. Li, G. Li, F. Dong, A. V. Kabashin, Z. M. Wang, *ACS Catal.* **2023**, *13*, 15546.
[202] a) S. Lian, M. S. Kodaimati, E. A. Weiss, *ACS Nano* **2018**, *12*, 568; b) S. Lian, M. S. Kodaimati, D. S. Dolzhnikov, R. Calzada, E. A. Weiss, *J. Am. Chem. Soc.* **2017**, *139*, 8931.
[203] J. A. Dirks, T. A. Williams, D. R. Brown, *J. Sol. Energy Eng.* **1992**, *114*, 254.
[204] W. H. Weber, J. Lambe, *Appl. Opt.* **1976**, *15*, 2299.
[205] a) M. J. Currie, J. K. Mapel, T. D. Heidel, S. Goffri, M. A. Baldo, *Science* **2008**, *321*, 226; b) F. Meinardi, F. Bruni, S. Brovelli, *Nat. Rev. Mater.* **2017**, *2*, 17072; c) R. Mazzaro, A. Vomiero, *Adv. Energy Mater.* **2018**, *8*, 1801903.
[206] N. D. Bronstein, Y. Yao, L. Xu, E. O'Brien, A. S. Powers, V. E. Ferry, A. P. Alivisatos, R. G. Nuzzo, *ACS Photonics* **2015**, *2*, 1576.
[207] L. R. Bradshaw, K. E. Knowles, S. McDowall, D. R. Gamelin, *Nano Lett.* **2015**, *15*, 1315.
[208] D. Mocatta, G. Cohen, J. Schattner, O. Millo, E. Rabani, U. Banin, *Science* **2011**, *332*, 77.
[209] R. R. Lunt, *Appl. Phys. Lett.* **2012**, *101*, 043902.
[210] L. Jin, E. Hamzehpoor, J. Liu, X. Liu, D. Benetti, G. S. Selopal, D. F. Perepichka, Z. M. Wang, F. Rosei, *J. Mater. Chem. A* **2023**, *11*, 23821.
[211] N. C. Giebink, G. P. Wiederrecht, M. R. Wasielewski, *Nat. Photonics* **2011**, *5*, 694.
[212] L. Xu, Y. Yao, N. D. Bronstein, L. Li, A. P. Alivisatos, R. G. Nuzzo, *ACS Photonics* **2016**, *3*, 278.
[213] R. Connell, C. Pinnell, V. E. Ferry, *J. Opt.* **2018**, *20*, 024009.
[214] H. Liu, S. Li, W. Chen, D. Wang, C. Li, D. Wu, J. Hao, Z. Zhou, X. Wang, K. Wang, *Sol. Energy Mater. Sol. Cells* **2018**, *179*, 380.
[215] A. Anand, M. L. Zaffalon, G. Gariano, A. Camellini, M. Gandini, R. Brescia, C. Capitani, F. Bruni, V. Pinchetti, M. Zavelani-Rossi, F. Meinardi, S. A. Crooker, S. Brovelli, *Adv. Funct. Mater.* **2019**, *30*, 1906629.
[216] A. Goetzberger, W. Greube, *Appl. Phys.* **1977**, *14*, 123.
[217] a) H. Zhao, D. Benetti, X. Tong, H. Zhang, Y. Zhou, G. Liu, D. Ma, S. Sun, Z. M. Wang, Y. Wang, F. Rosei, *Nano Energy* **2018**, *50*, 756; b) K. Wu, H. Li, V. I. Klimov, *Nat. Photonics* **2018**, *12*, 105; c) G. Liu, H. Zhao, F. Diao, Z. Ling, Y. Wang, *J. Mater. Chem. C* **2018**, *6*, 10059.
[218] A. R. M. Velarde, E. R. Bartlett, N. S. Makarov, C. Castañeda, A. Jackson, K. Ramasamy, M. R. Bergren, H. McDaniel, *ACS Appl. Energy Mater.* **2020**, *3*, 8159.
[219] C. Yang, D. Liu, R. R. Lunt, *Joule* **2019**, *3*, 2871.
[220] C. Yang, H. A. Atwater, M. A. Baldo, D. Baran, C. J. Barile, M. C. Barr, M. Bates, M. G. Bawendi, M. R. Bergren, B. Borhan, C. J. Brabec, S. Brovelli, V. Bulovic, P. Ceroni, M. G. Debije, J.-M. Delgado-Sanchez, W.-J. Dong, P. M. Duxbury, R. C. Evans, S. R. Forrest, D. R. Gamelin, N. C. Giebink, X. Gong, G. Griffini, F. Guo, C. K. Herrera, A. W. Y. H-Baillie, R. J. Holmes, S.-K. Hong, T. Kirchartz, et al., *Joule* **2022**, *6*, 8.
[221] H. B. Jalali, S. Sadeghi, I. Baylam, M. Han, C. W. Ow-Yang, A. Sennaroglu, S. Nizamoglu, *Nano Res.* **2021**, *14*, 1488.
[222] C. Li, W. Chen, D. Wu, D. Quan, Z. Zhou, J. Hao, J. Qin, Y. Li, Z. He, K. Wang, *Sci. Rep.* **2016**, *5*, 17777.
[223] D. C. J. Neo, W. P. Goh, H. H. Lau, J. Shanmugam, Y. F. Chen, *ACS Appl. Nano Mater.* **2020**, *3*, 6489.
[224] L. Dhamo, F. Carulli, P. Nickl, K. D. Wegner, V. D. Hodoroaba, C. Würth, S. Brovelli, U. Resch-Genger, *Adv. Opt. Mater.* **2021**, *9*, 2100587.
[225] H. Zhao, Y. Zhou, D. Benetti, D. Ma, F. Rosei, *Nano Energy* **2017**, *37*, 214.
[226] F. Purcell-Milton, Y. K. Gun'ko, *J. Mater. Chem.* **2012**, *22*, 16687.
[227] X. Zhang, H. Lv, W. Xing, Y. Li, C. Geng, S. Xu, *Nanotechnology* **2022**, *33*, 055602.
[228] O. Voznyy, L. Levina, J. Z. Fan, M. Askerka, A. Jain, M.-J. Choi, O. Ouellette, P. Todorović, L. K. Sagar, E. H. Sargent, *ACS Nano* **2019**, *13*, 11122.
[229] Y. Han, B. Tang, L. Wang, H. Bao, Y. Lu, C. Guan, L. Zhang, M. Le, Z. Liu, M. Wu, *ACS Nano* **2020**, *14*, 14761.
[230] Z. Xiao, Z. Song, Y. Yan, *Adv. Mater.* **2019**, *31*, 1803792.
[231] H. Lv, C. Wang, G. Li, R. Burke, T. D. Krauss, Y. Gao, R. Eisenberg, *Proc. Natl. Acad. Sci. U. S. A.* **2017**, *114*, 11297.
[232] L. Shi, D. Benetti, F. Li, Q. Wei, F. Rosei, *Appl. Catal., B* **2020**, *263*, 118317.
[233] R. Akilimali, G. S. Selopal, D. Benetti, M. Mohammadnezhad, H. Zhao, Z. M. Wang, B. Stansfield, F. Rosei, *Catal. Today* **2020**, *340*, 161.
[234] Q. Y. Chen, Z. C. Wang, K. Q. Chen, Q. Fu, Y. L. Liu, Y. P. Zhang, D. L. Li, C. X. Pan, *RSC Adv.* **2019**, *9*, 33747.
[235] G. S. Selopal, M. Mohammadnezhad, F. Navarro-Pardo, F. Vidal, H. Zhao, Z. M. Wang, F. Rosei, *Nanoscale Horiz.* **2019**, *4*, 404.
[236] G. S. Selopal, R. Chahine, M. Mohammadnezhad, F. Navarro-Pardo, D. Benetti, H. Zhao, Z. M. Wang, F. Rosei, *J. Power Sources* **2019**, *436*, 226849.
[237] J. Wang, Y. Yuan, H. Zhu, T. Cai, Y. Fang, O. Chen, *Nano Energy* **2020**, *67*, 104217.
[238] X. Liu, D. Benetti, F. Rosei, *J. Mater. Chem. A* **2021**, *9*, 23345.
[239] L. J. Brennan, F. Purcell-Milton, B. McKenna, T. M. Watson, Y. K. Gun'ko, R. C. Evans, *J. Mater. Chem. A* **2018**, *6*, 2671.
[240] A. M. Saeboe, A. Y. Nikiforov, R. Toufanian, J. C. Kays, M. Chern, J. P. Casas, K. Han, A. Piryatinski, D. Jones, A. M. Dennis, *Nano Lett.* **2021**, *21*, 3271.
[241] G. J. Stasiuk, S. Tamang, D. Imbert, C. Gateau, P. Reiss, P. Fries, M. Mazzanti, *Dalton Trans.* **2013**, *42*, 8197.
[242] K. M. Tsoi, Q. Dai, B. A. Alman, W. C. W. Chan, *Acc. Chem. Res.* **2013**, *46*, 662.
[243] S. Nikazar, V. S. Sivasankarapillai, A. Rahdar, S. Gasmi, P. S. Anumol, M. S. Shanavas, *Biophys. Rev.* **2020**, *12*, 703.

Lei Jin received her Ph.D. degree from the National Institute of Scientific Research in 2019. She was a Joint Postdoctoral at National Institute of Scientific Research and McGill University from 2019 to 2023. Now she is a SUSTech Presidential Postdoctoral Fellow at Southern University of Science and Technology. Her research interests include nano optoelectronic devices utilizing nanomaterials including QDs, 2D materials, and carbon materials.

Gurpreet Singh Selopal received his Ph.D. degree at the University of Brescia, Italy. He is currently an Assistant Professor in the Department of Engineering, Faculty of Agriculture at Dalhousie University, Canada. His research work is primarily focused on the design and optimization of nanostructured materials to develop high-performing sustainable energy conversion/storage, environmental remediation, and smart agriculture technologies.

Xin Tong obtained his B.E. degree in Electronic Science and Technology (2014) and Ph.D. degree in Materials Science and Engineering (2018) from the University of Electronic Science and Technology of China (China). He is currently a professor at University of Electronic Science and Technology of China. His research interests focus on the design and synthesis of colloidal QDs and their applications in optoelectronics.

Dmytro (Dima) Perepichka is a William MacDonald Professor of Chemistry at McGill University, Montreal. He obtained his PhD in 1999 from the Institute of Physical Organic & Coal Chemistry in Donetsk (Ukraine) and worked as a post-doctoral fellow at the University of Durham and UCLA. He started his group at INRS in Varennes, Canada in 2003 and moved to McGill in 2005. His group focuses on synthetically driven research in π-electron functional materials, including small molecules, polymers, and 2D materials, aimed at understanding their behavior in optoelectronic devices.

Zhiming Wang, Dean of the Institute of Fundamental and Frontier Sciences (IFFS) at the University of Electronic Science and Technology of China (UESTC), National Leading Talent, Fellow of the Optical Society of America (OSA, currently Optica), Fellow of the Royal Society of Chemistry (RSC). His research focuses on the fundamental applications of micro and nanostructures in the cross-cutting frontiers of integrated photonics, quantum technology, flexible electronics, and renewable energy. Currently, he is in charge of a National Key Research and Development Program of China and and an Overseas Expertise Introduction Center for Discipline Innovation.

Federico Rosei studied Physics (PhD 2001) at the University of Rome "La Sapienza", Italy. Currently, he holds the Chair of Industrial Chemistry at the Department of Chemical and Pharmaceutical Sciences, University of Trieste, Italy. His research interests focus on structure/property relationships in nanomaterials and their use as building blocks in emerging technologies.